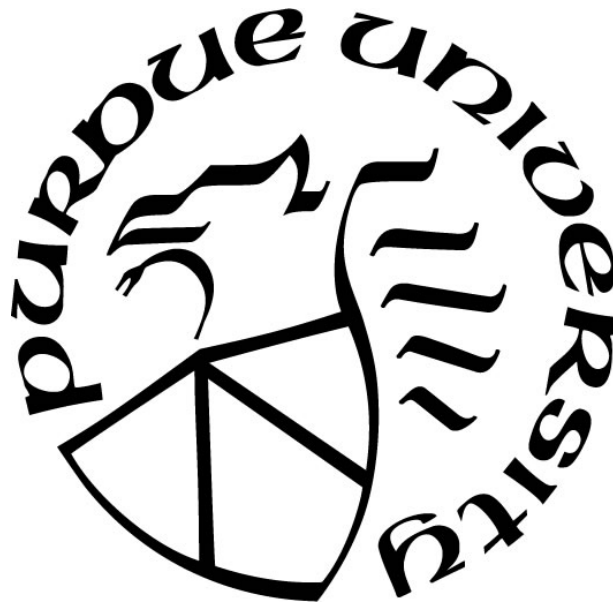# THE COMPUTATIONAL FLUID DYNAMIC SIMULATION OF SLAB SURFACE SCALE FORMATION DURING REHEATING PROCESS

by

Xiang Li

A Thesis

Submitted to the Faculty of Purdue University

In Partial Fulfillment of the Requirements for the degree of

Master of Science in Mechanical Engineering

Department of Mechanical and Civil Engineering

Hammond, Indiana

December 2021

THE PURDUE UNIVERSITY GRADUATE SCHOOL
STATEMENT OF COMMITTEE APPROVAL

Dr. Chenn Q. Zhou, Chair

Department of Mechanical and Civil Engineering at Purdue Northwest

Dr. Xiuling Wang

Department of Mechanical and Civil Engineering at Purdue Northwest

Dr. Ran Zhou

Department of Mechanical and Civil Engineering at Purdue Northwest

Approved by:

Dr. Xiuling Wang

To my parents

TABLE OF CONTENTS

LIST OF TABLES

LIST OF FIGURES

LIST OF SYMBOLS

Symbol	Description	Symbol	Description
x	Thickness of the scale	t	Time
k_l	Linear rate constant of scale formation	$a_{O,i}$	Oxygen activity in wüstite at wüstite/i interface
a_O	Oxygen activity	m	Exponent of oxygen activity
p	Partial pressure of oxidant	p_i	Partial pressure of i
$(\Delta m/A)$	Weight increase per unit area	K	Rate factor
q	A constant	K_i	The ith rate factor
t_η	Time at time step η	p	Time difference between time steps
a, b	Constants	e	Base of natural logarithm
M, B	Constants	O/Fe	Oxygen/iron atom ratio
Me	Assumed oxidizing metal	ζ, η	Thicknesses of layers
w, y	Constants in reaction	v, δ	Metal/oxygen ratio in Me oxide
K_p	Thickness change ability constant	Z, Z_O	Valence of metal and oxygen
P', P''	Partial pressure of oxygen at boundaries of scale	k_0	Thermal conductivity
T_i	Temperature at surface of phase i	D_i	Diffusion coefficient of i
ρ	Density	$\vec{v}$	Velocity vector
$\bar{\bar{\tau}}$	Stress factor	$\vec{g}$	Gravity acceleration
I	Unit tensor	k_{eff}	Effective thermal conductivity
$\bar{\bar{\tau}}_{eff}$	Effective stress tensor	$\vec{J}_j$	Diffusion flax of species j

S_h	Heat source term	H	Enthalpy
C_p	Constant-pressure specific heat	u	Velocity component
x	Direction component (only in turbulence equation)	μ	Molecular viscosity
μ_t	Turbulent viscosity	G_k, G_b	Turbulence kinetic energy
Y_M	Contribution of the fluctuating dilatation	$\vec{r}$	Position vector
$\vec{s}'$	Scattering direction vector	a	Absorption coefficient
σ_s	Scattering coefficient	I	Radiation intensity
σ	Stefan-Boltzmann constant	Φ	Phase function
Ω'	Solid angle	$a_{\varepsilon,i}$	emissivity weighting factor for the ith fictitious gray gas
K_i	Absorption coefficient of the ith gray gas (only in WSGGM)	p	The sum of the partial pressures of all absorbing gases (only in WSGGM)
S	Path length	Y_i	Mass fraction of species i
R_i	Net rate of production of species i	S_i	Sources of rate of creation
$\Delta G°$	Standard Gibbs free energy	k_p	Parabolic rate constant
$k_{l,i}$	Linear rate constant of species i	M_i	Molar weight of species i
E_i	Heat of activation of reaction with species i	β	Factor of mass transfer coefficient of gas flow
Re	Reynold number	Sc	Schmidt number
R	Gas constant	γ_i	Iron ion vacancy concentration at boundary i
ρ_i	Density of species i	r_i	Thickness fraction of species i
H	Formation heat	ΔH_O	Reaction heat per molar oxygen atom
ΔH	Total reaction heat	Q	Transferred heat
k_i	Thermal conductivity of i	l	Length or depth

ABSTRACT

Reheating furnace is a furnace that using fuel combustion energy to heat steel products before hot rolling. Materials need to reach the temperature around 1400K uniformly after heating in reheating furnaces. Steel oxidizes during the reheating process. Oxidize scale layer on the surface will changed the heat transfer properties of surface and increase the inner stress of material, reducing the quality of the steel. In this study, a model of scale formation under reheating furnace working condition is developed. The model can be coupled into computational fluid dynamics (CFD). The commercial software, ANSYS FLUENT®, was utilized to give a prediction of furnace atmosphere and calculate the formed scale. A calculator is also developed to predict the scale formation of a single point during the reheating process using measurable flow field data. Furthermore, a series of parametric studies has been investigated to study the influence of operating conditions.

1. INTRODUCTION

1.1 Reheating Furnace in Steel Making

Reheat is the first step of the hot rolling process, in which steel products are heated in the reheating furnace to make the metal more malleable for rolling [1]. Higher rolling temperatures lead to a lower metal rolling force requirement but also cause structural damage due to thermal stress. For steel, the temperature used for most grades and furnace is between 1200°C and 1250°C. As shown in Figure 1-1, the microstructure of most of the steel changed into austenite, and steel with higher carbon content and cast iron are starts to liquefy at these temperatures. Alloy elements on the surface also can be melted and fused into the steel slab to form a more uniform distribution during the reheating process [1]. And internal stress caused by casting can be relived because of the structure changing and temperature raising of the material.
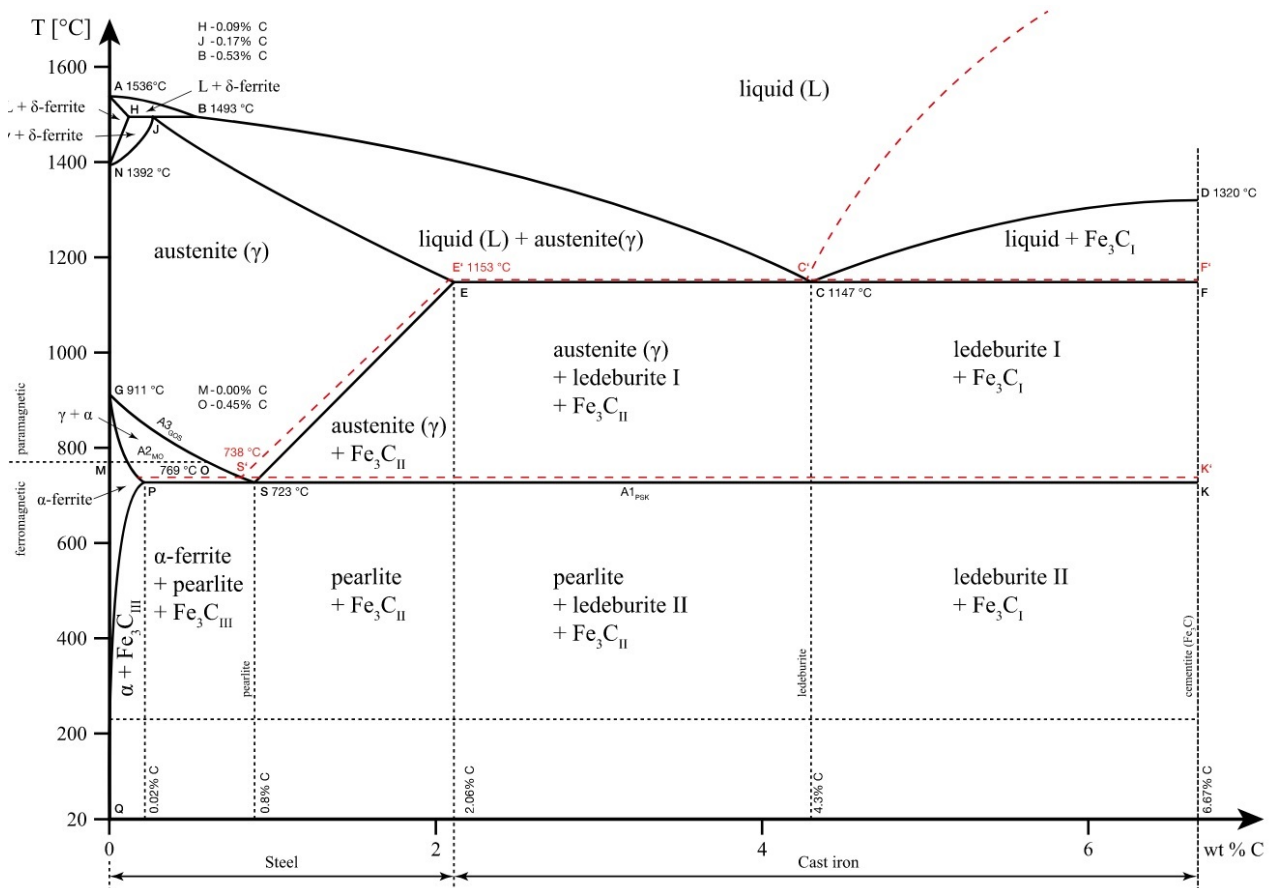

Figure 1-1. Iron carbon phase diagram [2]

Several different purposes can be given to a single furnace. For the hot rolling process to produce a high-quality product, a uniform rolling through the whole process is required. The rolling force is highly related to the structure of the steel, which is temperature-sensitive. To achieve the goal of the rolling process, the main objective of the reheating furnace, form an even temperature distribution throughout the slab is necessary. Minor goals most concentrate on improving the efficiency like reducing fuel and energy cost exhaust gas energy recovery, and environmental protection such as minimizing emissions. All of these factors are controlled by the combustion process inside the reheating furnace.

Two types of steel reheating furnaces that are normally used by large rolling mills are distinguished by the type of slab motion. Pusher-type furnaces move slabs by the semi-continuous charging of succeeding slabs into the furnace. The walking-beam furnace uses a movable beam structure to lift and move the slab to the next position regularly to transport slabs through the furnace. Except for the moveable walking beam, there are beams inside both two types of furnace to hold slabs, commonly called skids. Colling water flows inside skids to avoid heating damage to the skid. However, the cooled skids cause skidmarks on the bottom of the slab by absorbing more convection and radiation heat from slabs.

Reheating furnaces are divided into several zones to reach different purposes. For example, a pusher type furnace is shown in Figure 1-2. Slabs charged from the left side of the furnace and near the furnace charge door is a non-flame area. Because of the structure of reheating furnace, hot gas from combustion will flow forward to this area and warm up cold slabs. Then the first zone is the preheat zone where slabs are slowly heated. And slabs reach the target temperature in the heating zone and are then moved to the soaking zone. Slabs are kept heated in the soaking zone to make sure the core is heated up to make the whole product temperature uniform. The outlets of the flue gas are set in the non-flame area before preheating zone. Energy recovery can be applied to exhausted gas by using flue gas to heat oxide gas to improve efficiency and raise the flame temperature. The slab left soaking zone is then discharged to the scale removing and be rolled in the rolling machine.

The combustion process is the most important part of the reheating furnace. In Fig 1.2, the combustion mainly happens in the gray area in the figure, fuels are injected from the burner on the furnace wall and react with oxidant, most commonly used is air, to form a flame. Heat is transferred from flame to the product through two main ways, convection and radiation. Around 90-95% of

heat is transferred by radiation, and the other part is from the convection on the contacting surface of products and hot gas [3][4]. As mentioned before, in most of the reheating furnaces, combustion product flow direction near products surface are opposite to the products moving direction. Since the convection cannot fully transfer heat in the gas to the slab, flue gas that still contains a large amount of energy exhaust through the outlets, charge door and discharge door. Gas left from the charge door and discharge door are wasted, but the energy in gas exhausted through the outlet is still possible to be recovered.
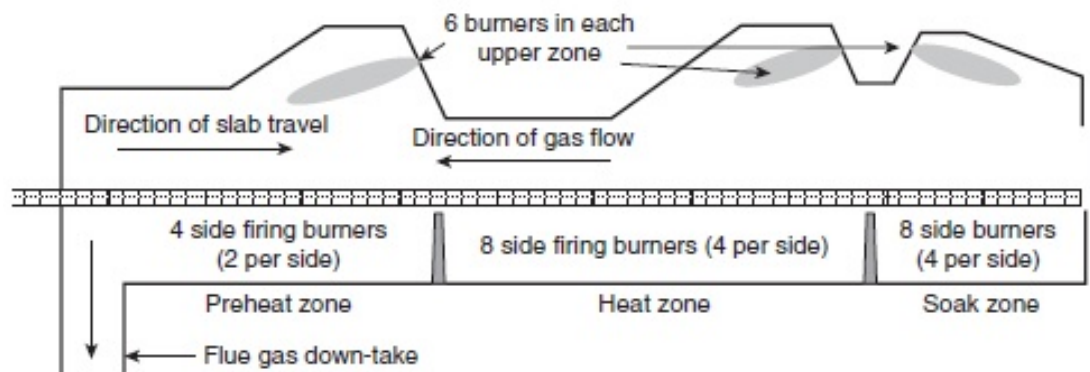
Figure 1-2. Structure of a pusher type reheating furnace [1]

The most important objectives of the combustion are providing enough heat to the products and avoiding high-temperature flame damage the wall of the reheating furnace. Since most of the heat is transferred through the radiation which is highly related to the radiation source temperature, the flame temperature is required to be high enough to achieve a high-efficiency heat transfer. But an unnecessary high flame temperature can overheat the product and furnace wall and cause damage. And a high-temperature flame too close to the wall can also damage the furnace wall. So the control of flame temperature and position is also needed. Besides two objectives that must be accessed, ancillary goals include reducing the fuel cost and reducing pollutant gas emissions.

Since the fuel consumption, energy generation and transfer are all through combustion, the improvement of the combustion process is a feasible way to reduce the cost of fuel and energy. Preheat oxidant using recuperative or regenerative processes on the flue gas is a commonly implemented method to both improve the combustion efficiency and reduce energy waste. Control of the combustion process itself is also important. The most common fuel of reheating furnace is methane, chemical formula CH_4. Although nitrogen in the air can also react with oxygen to form

nitrous oxides, normally this reaction is ignored in the global reaction. So the global reaction of methane fully combustion with air is:

$$CH_4 + 2(O_2 + 3.76N_2) \rightarrow CO_2 + 2H_2O(g) + 7.52N_2 \tag{1.1}$$
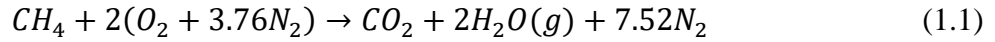
Where the nitrogen does not influence the chemical process except being a diluent. On the reactant side, nitrogen reduces the chance of methane molecules meeting oxygen molecules, improves the oxygen requirement. Because of the influence of nitrogen, product and turbulent mixing, although stoichiometric have the best theoretical efficiency, some extra air is required for methane to fully react. On the product side, the nitrogen absorbs reaction heat to increase the temperature to be the same as the other products, which decreases the average product temperature and flame temperature. Several ways based on the basic chemical formula can be considered to improve combustion efficiency. Such as improving the mixing to reduce the excess air requirement, or improving the oxygen fraction to more than 21% in the oxidant. Both two ways can improve the reaction rate by making methane meet oxygen easier and reducing heat wasted on heating gas by reducing the total amount of gas at the same time.

The combustion process has many steps and produces carbon monoxide, carbon dioxide and nitrogen oxides as part of products. These products are pollutants that must be controlled. Carbon monoxide is the product of incomplete combustion and carbon dioxide pyrolysis. Nitrogen oxides are mainly formed by the combination reaction of nitrogen and oxygen under high temperatures. So control the maximum temperature is a common way to reduce pollutant emissions.

1.2 Scale Formation

Some oxidants are also contained in the products, including excess O_2 and water vapors, CO_2 can also be an oxidant at high temperatures. They react with the iron and alloy on the steel surface and can form an oxide layer on the surface with several millimeters of thickness. These oxidized metal formed in the reheating furnace is called the primary scale. The compositions of the scale include FeO, magnetite, hematite and furnace gas inside the cavities of oxides. These scales have lower thermal conductivity and change the heat transfer contribution of the slab.

1.3   Objective

The objective of this research is to develop a scale formation model and to apply the model to the numerical simulation of the reheating furnace. Since numerical simulation can provide a large amount and range of types of flow field data, the scale formation model needs to consider different variables instead of only depending on temperature.

2. LITERATURE REVIEW

2.1 Simulation of Reheating Furnace

The reheating furnace is quite complex, it's costly to do the necessary experimental test for an operation improvement using an actual reheating furnace due to the downtime and time required for the tests. As such, many researchers have turned to computational methods to study the reheating furnace and the influence of different operating conditions. Some tests that have an unacceptable cost as a test on the real furnace such as changing the fuel can also be easily done using computational method. While many of the computational methods are using simplified models based on the experimental result, through adequate validation, these methods can still provide a reliable prediction of the result of the reheating process. Computational needs to build a domain that describe the floating field area and discretize the given domain into much smaller spatial and temporal elements in order to solve the conservation equations for mass, momentum, energy and various properties. The accuracy of the computational method depends on the size and resolution of the elements in the domain, a fetter meshing of elements normally resulting in a more accurate result. The combination of all the elements in a given domain is called the mesh.

Modeling of reheating furnace over experimental work rely on small-scale trials and large-scale implementation has several limits. A small-scale trial using an experimental furnace cannot model all the effects of a changed operation accurately, and the cost of material, downtime and testing time also can't be avoided. The testing using the whole furnace may require more downtime and testing time to solve problems met and the quality of products may be lower during the test. The application of an operation without fully ensuring its effectiveness may result in erroneous implementation and reduce productivity. For numerical methods, theoretical and experimental knowledge is used to predict the result of the operation, and the main cost is the computational demand and time. Thanks to modern computing technology, the efficiency of numerical calculation is keep rising and the cost keeps reducing [5].

Same with the experimental work, the study of reheating furnace using numerical simulation consist of the whole furnace modeling and research of discrete phenomena, such as turbulence and heat transfer. Simplified models, such as well-stirred reactor, have been used to predict specific parameters like total heat rate or heat flux [6], and test the accuracy of sub-models

of the furnace model. Since numerical methods such as computational fluid dynamic (CFD) are computationally expensive, the usage of simplified methods improves the efficiency of distribution solving of specific parameters.

Hottel and Sarofim. simplified the furnace into a well-stirred reactor to study the influence of using different radiation models and parameters in 1970 [6]. The well-stirred reactor model assumes the temperature and gas consistent of a single zone are all the same everywhere. Although mixing and temperature distribution are all ignored in the model, but Hottel and Sarofim. confirmed that gray-gas radiation models work better compare with simpler models. Li et al. mathematically modeled the reheating furnace in 1988 [3]. They found that the radiative shielding of skids is the main reason of the formation of skidmarks. Chapman et al. developed a 2D model with more complex turbulence, combustion and radiation models than previous studies [4]. They combined the weighted-sum-of-gray-gases method and discrete ordinates method to model the radiation of furnace gases. They found that 88-93% of total heat flux to the slab is transferred through radiation. It's also found that most of the energy losses are through flue gases.

Kim et al. modeled a 3D steel reheating furnace in 2000 [7]. This steady-state model assumed the furnace can reach a state that reaches a balance and won't change with time to reduce the computational cost. The turbulence, combustion, heat transfer and NO_x generation are considered in the model. They also analyzed the heat flux to the slab and got a similar finding with Chapman et al. that radiation transfer 94.2% of the total heat to the slab. And they also gave a furnace efficiency value of 37.7%.Yang et al. combined slab reheating with the gas flow field [8]. The static slab transfers its temperature data from a coordinate to the next one within a specific speed to simulate the motion of the slab until the temperatures distribution of the slabs does not change anymore. Huang et al. coupled slab motion with flow field by considering the steel as laminar flow without reaction and radiation [9]. Slab temperature distribution during the whole reheating process can be predicted by both these methods.

One important factor that needs to be considered in computational studies is the computational ability and resources. Although mesh sizing can decide the accuracy of the simulation result, it still needs to consider both the size of the domain and the computational resources available. Various methods can couple the slab motion, slab heating, flow field and combustion together, the most direct way is to build the full furnace domain transiently with a dynamic mesh to describe slab motion. But this method requires remeshing at every time step

which requires much more resources than the steady-state method. To solve the cost problem, some numerical software has been developed functions such as "overset mesh" or "mesh motion" that can avoid rebuilding mesh in the transient method. And some indirect approaches like previously mentioned methods of Yang et al. and Huang et al, using a steady-state mesh and transferring their temperature data using settings or laminar flow to reduce the computational cost.

Computational fluid dynamics (CFD) is a branch of fluid mechanics that uses numerical analysis and data structures to analyze and solve problems that involve fluid flows. Computers are used to perform the calculations required to simulate the free-stream flow of the fluid, and the interaction of the fluid with surfaces defined by boundary conditions. Benefit from the development of computing technology, CFD is widely used in industry to analyze fluid flow, heat transfer, combustion and other parameters inside the equipment. So couple the scale formation into CFD analysis are studied by some researchers in recent years. Schluckner et al applied a scale formation model to analyze the impact of different combustion atmospheres, including air-fuel combustion and oxygen-enriched combustion, on the scale formation rates in a natural gas-fired lab-scale furnace [10]. The research found that the material losses aroused by scale formation can be decreased by using the oxygen enrichment combustion due to the increased heat transfer decrease the re-heating time. Liu et al introduced a simplified numerical method to simulate scale formation and apply it to a three-dimensional numerical model of a pusher-type reheating furnace and successfully works in the CFD simulation [11]. Worl chose to use the method of Abuluwefa to build a numerical model and coupled it with CFD simulation, model is validated and used in her thesis [12]. The thesis work builds upon the work by Worl. It can be also seen as the further improvement of Worl's thesis work.

2.2   Scale formation

2.2.1   Oxidation of steel

Oxidation is a very complex phenomenon that has a large influence on the high temperature process, especially the process of metals that can be oxide such as steel and iron. It's hard to totally avoid oxidation, and metal can form several types of oxides during the process. These oxides cause the property changing and waste of the material, which reduce both the quality and efficiency. The example in study is that when the steel are being reheated, it need to be heated up inside the

reheating furnace at around 1250℃ for 1-2 hours. The metal total volume lost because of steel oxidation is 1-2%. Scale may split from steel slab and required downtime to clean. As such, analysis of scale and its formation has continued to be an area of interest for researchers.

By measuring the temperature corresponding to the position of the sharp boundary between phases, Dark and Gurry obtained the CO_2/CO ratio in equilibrium with iron and wüstite, which means at the boundary of iron and wüstite, at temperature from 1038 to 1365 °C, and that in equilibrium with wüstite and magnetite from 1096 to 1388 °C [13]. The two ratios of H_2O/H_2 are also obtained using the same method. Pettit and Wagner found the linear reaction rate of steel oxidation in the temperature interval 700-1000 °C in CO_2 and CO mixtures base on the surface reaction rate controlled method [14].The CO_2/CO ratio at the boundaries was found can decide the CO_2 transfer rate inside the wüstite and influence the maximum rate of CO_2 reaction rate at the surface. They also found that for larger oxide thickness the oxidation rate changed into a parabolic rate from the experimental data. The method of Pettit and Wagner then be used on the explanation and calculation the steel oxidation in the mixture of water vapor and hydrogen by Turkdogan et al [15]. They used the microsection like Figure 2-1 doing the measure the scale thickness and found that the initial part of the iron oxidation, the reaction rate in water vapor-hydrogen gas mixtures is higher than that in carbon dioxide-carbon monoxide mixture. Grabke et al did the further study on steel oxidation in CO_2 and H_2O [16]. In the previous studies, equation of linear scale thickness growth rate is:

$$dx/dt = k_l a_{O,iron}{}^{-m}(1 - a_{O,iron}/a_{O,gas})p \qquad (2.1)$$

x is the thickness of the scale, t is the time, k_l is a linear rate constant, p is the partial pressure of oxidant, $a_{O,iron}$, $a_{O,gas}$ are the oxygen activity in wüstite at wüstite/iron and wüstite/gas interface, the oxygen activity can be calculated using equation:

$$a_O = p_{oxidant}/p_{reduction\ product} \qquad (2.2)$$

Use CO_2 as an example:

$$a_O = p_{CO_2}/p_{CO} \qquad (2.3)$$

m is the exponent of oxygen activity, before Grabke, the m value directly set to $-2/3$, Grabke et al. propose that the exponent m is changing with temperature [16].
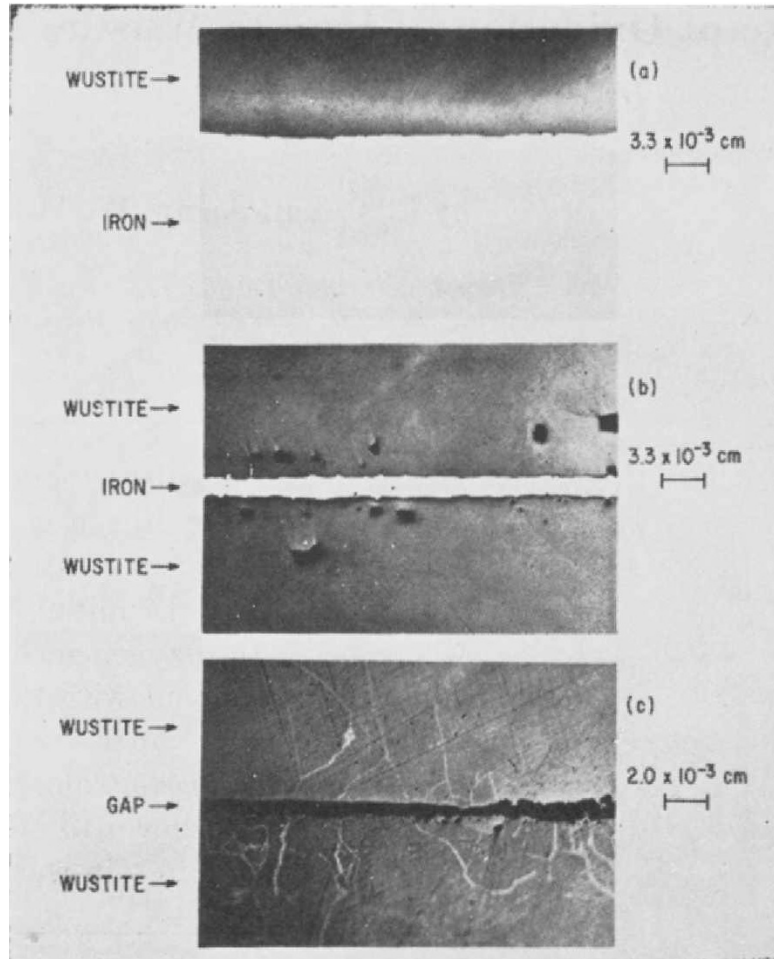
Figure 2-1 Microsections of iron-wüstite interface after oxidation of iron
in $H_2O - H_2$ mixture [15]

In 1970, Sachs and Tuck studied the scale formation in gas with a composition similar to the environment gas during reheating [17]. A method using rate constant to describe both linear rate and parabolic rate is developed. The main equation of the method is:

$$(\Delta m/A)^q = Kt \tag{2.4}$$

$(\Delta m/A)$ is the weight increase per unit area, K is the rate factor and q is a constant. When $= 1$, the equation represent the linear rate of the scale formation, and when $q = 2$, the equation represent the parabolic rate constant. A semi-graphical method of evaluation is used for the rate factor K calculation. A group of known time and isothermal scaling constant data is used to plot a graph of scaling constant against time as shown in Figure 2-2. Here p is a small time increment during which the scaling constant changed from K_0 to K_1.

Figure 2-2 Plot of scaling constant K against time t [17]

While the value of p is smaller enough, when transforming the plot into one of lnK versus t, the curve between t_η and $t_{\eta+1}$ can be simplified to a straight line as shown in Figure 2-3.
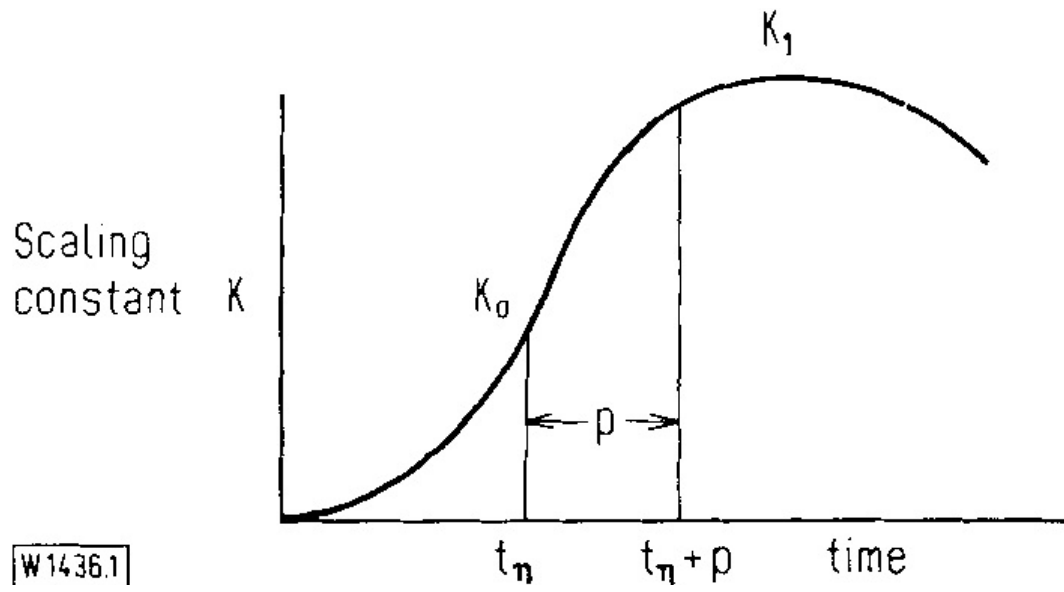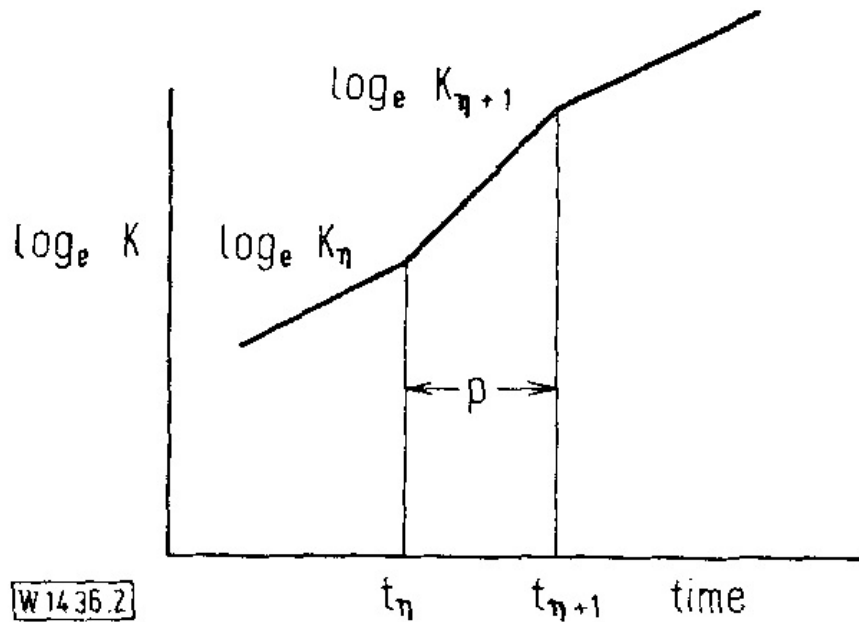

Figure 2-3 Plot of lnK against time t [17]

Then K is written as:

$$K = be^{at} \tag{2.5}$$

At a constant temperature in an atmosphere with a stable consistent, a and b are constants. So from known K_η and $K_{\eta+1}$, a and b can be determined by equations:

$$a = (lnK_{\eta+1} - lnK_\eta)/\text{p} \qquad (2.6)$$
$$b = K_\eta/e^{at_\eta} \qquad (2.7)$$

The method can do the predict base on the experimental data, but a large number of sample testing is still required for the theory.

Deich and Oeters developed a method of linear rate constant of oxidizing by oxygen based on the gas transport controlled theory in which the maximum reaction rate of oxidation depends on the oxygen transportation rate from gas to the slab surface [18]. An iron ion transport theory is used to describe the parabolic reaction rate. The ion transport theory thinks that iron ions react with the oxygen at the surface generating the scale. To reach an equilibrium of surface ion concentration, the reaction rate needs to be the same with or lower than the maximum transfer rate of iron ions from the iron/scale interface to the surface of the scale. Along with the increase of the scale thickness, the transfer rate of ions decreases and form a parabolic curve of scale thickness against time. And when the surface reaction rate is slower than the maximum ion transfer rate, the gas transport controlled theory thinks that the oxygen near the slab surface is easy to be fully reacted. And to reach the atom equilibrium, the oxidation reaction rate cannot be faster than the transport rate of oxygen from the bulk of the gas.to the reaction surface. Since the oxygen transportation in the gas is not related to the scale property, it won't change with the scale thickness or time, so this theory is one of the explanations of the linear rate of steel oxidation.

A study about scale formation in furnace atmosphere with excess air which considering oxygen, carbon dioxide and water as oxidizers was done by Abuluwefa in 1992[19]. A summarize of previous theories and a study of the influence of different parameters have been made and experiments and calculations of scale formation have been done in the study. According to the iron oxygen diagram shown in Figure 2-4, the main consistent of scale are wüstite and magnetite. In the study, steel is assumed as pure iron and scale is assumed to consist of 95% wüstite and 5% magnetite. A 35% reduction of scale formation while the excess air decreased from 70% to 20%, and excess amounts of scale formed at higher temperature or while having longer residence time are found in the study.

RATIO O/Fe
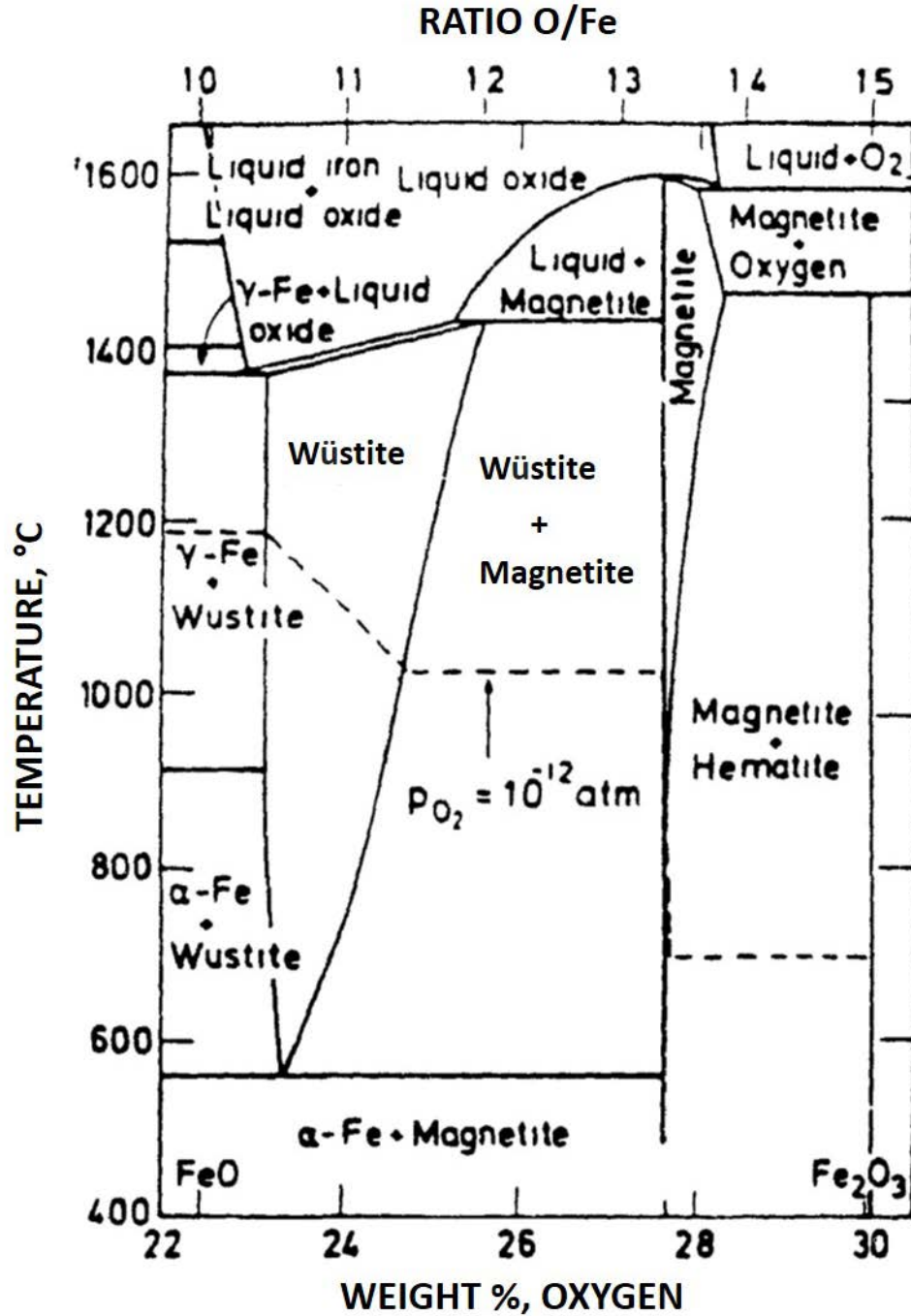
Figure 2-4 Iron oxygen phase diagram [19]

More experiments have been done by Abuluwefa et al to examine the predicted oxidation rate on the basis of previous oxidation mechanisms [20][21]. Oxidation in different atmospheres at different temperature have been tested, for example, the result of steel oxidation in the atmosphere consists of 1% O_2, 10% CO_2, 3% H_2O and 86% N_2 are shown in Figure 2-5.

Abuluwefa et.al found that the controlling mechanism in the oxidation of low carbon steel during reheating in the industrial reheat furnace was intermediate between linear and parabolic, where the linear mechanism predominated.
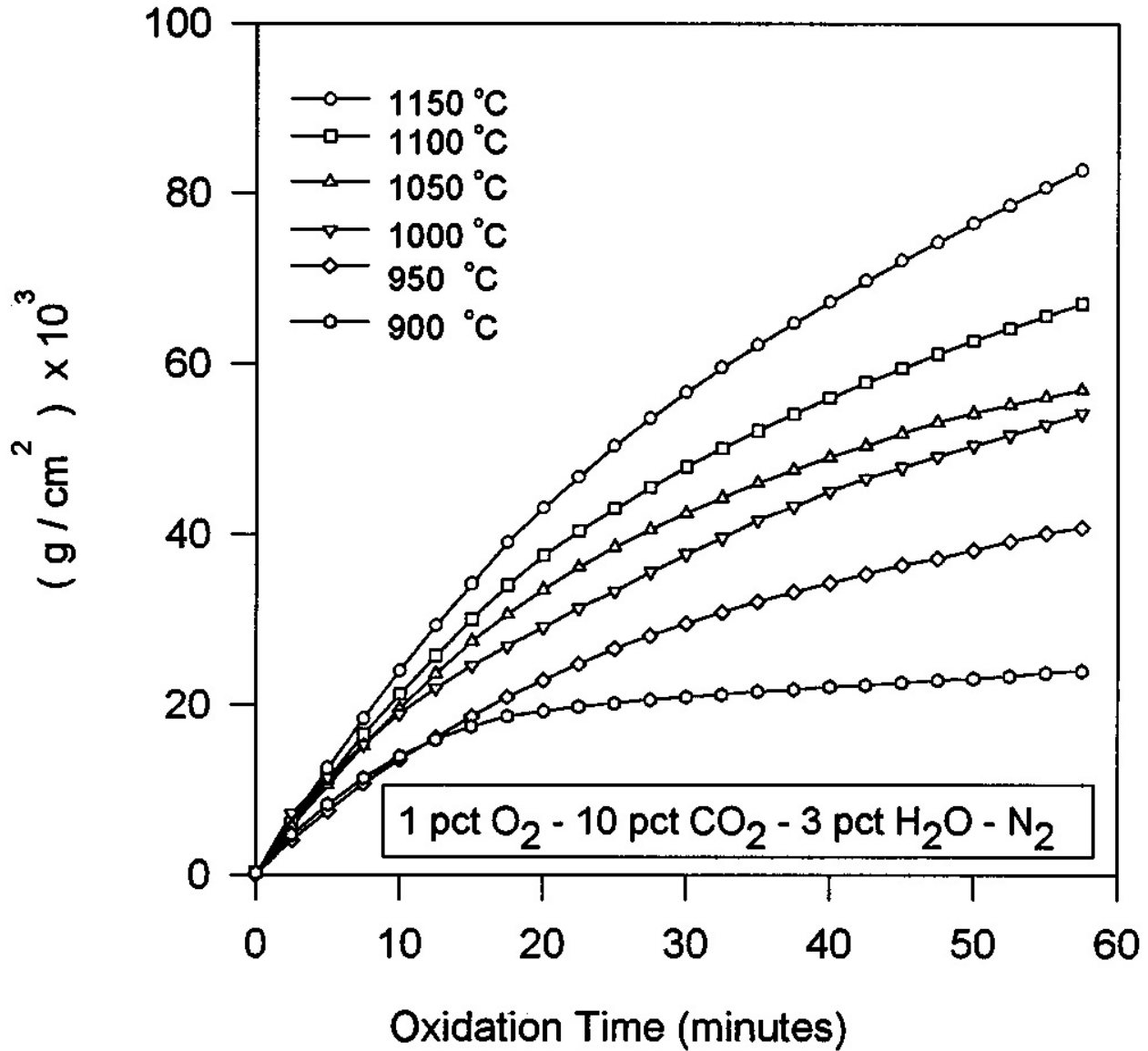
Figure 2-5 Experimental result of oxidation in 1% oxygen atmosphere [21]

Chen and Yuen find that the calculated linear rate constant is smaller than the experimental result in literatures using small samples [22]. It's found that one assumption of all theories is the product surface is a semi-infinite space, but samples used for experimental studies are only several centimeters long and can't be considered as semi-infinite plates, so the influence of edge effect

and gas flow rate differences increase the scale formation rate. As a result of the research, some factors are introduced for calculating the linear rate constant.

Some of the important parameters used in scale formation prediction are studied by different researchers. Giddings and Gordon reviewed the oxygen activities and phase boundary in wüstite [23]. The experimental oxygen potentials are summarized into an equation with the scale composition:

$$\log P_{O_2} = M(O/Fe) + B \tag{2.8}$$

P_{O_2} is the oxygen potential, M and B are constants, and O/Fe represents the composition of the scale. The value of parameters is shown in Table 2-1 Analysis of composite and boundary data for P_{O_2} Table 2-1.

Table 2-1 Analysis of composite and boundary data for P_{O_2}

Temperature (°C)	M	B	O/Fe at $Fe - Fe_xO$ boundary	O/Fe at $Fe_xO - Fe_3O_4$ boundary
700	21.447	-44.078	1.0555	1.0939
800	22.191	-42.211	1.0538	1.1133
900	22.808	-40.663	1.0525	1.1294
1000	22.328	-39.357	1.0514	1.1432
1100	23.772	-38.242	1.0506	1.1552
1200	24.155	-37.298	1.0500	1.1666
1300	24.491	-36.437	1.0492	1.1753

Chen and Peterson developed a method to express the self-diffusion coefficient of Fe in wüstite [24]. Yin et al further research the oxidation of low carbon steel in gas consist of N_2-H_2-H_2O [25]. The research confirms that at 1100°C, the linear rate is controlled by an oxide-gas interfacial process, with an effective activation energy of less than 80kJ/mol. But this surface-reaction controlled method was not observed at lower temperatures like 800°C, and linear scale formation rate is controlled by gas transport at such temperature. Lee et al studied the steel oxidation in different gas generated from fuel-air mixtures with different fractions [26]. The air-fuel ratio, which is the actual air in the mixture compared with the stoichiometrically required for fully combustion, is used to describe the concentration of the mixture. The result of equilibrium partial pressure is measured and shown in Table 2-2. Scale formation rate is calculated based on the partial pressures, and it's found that in the range of air-fuel ratio from 95% to 112%, since the

excess oxygen in the mixture is too less and oxygen partial pressure in the combusted gas is low, the reaction rate is highly influenced by the concentration of carbon dioxide and water vapor.

Table 2-2 Equilibrium Partial Pressures (atm) of Reaction Gases [26]

Air-fuel ratio (%)	CO_2	CO	N_2	O_2	H_2O	H_2
112	8.57×10^{-2}	3.5×10^{-7}	0.72	2.1×10^{-2}	0.171	3.5×10^{-7}
108	8.86×10^{-2}	4.4×10^{-7}	0.72	1.4×10^{-2}	0.177	4.4×10^{-7}
101	9.42×10^{-2}	1.3×10^{-6}	0.72	1.9×10^{-3}	0.188	1.3×10^{-6}
99	9.38×10^{-2}	1.9×10^{-3}	0.71	8×10^{-10}	0.190	1.9×10^{-3}
95	8.90×10^{-2}	9.6×10^{-3}	0.70	3×10^{-11}	0.187	1.0×10^{-2}

2.2.2   Scale separation

As shown in Figure 2-4, at around 900°C, the microstructure of the steel starts the changing from α phase to γ phase. During the process, the dimension of the slab also changed with the phase changing. But the scale layer contains magnetite and hematite which are comparatively harder than wüstite and steel, so the scale layer cannot easily change the shape to fit the slab dimension changing [27]. At some part, the scale is separate from the slab surface and leave a gas gap between the scale layer and slab surface, and some gas gaps may also form between the wüstite and magnetite layer. All these separations change the iron ion transfer property and change the formation rate of the scale.

Sachs and Tuck noticed that the separation decreases the scale formation rate in the nonisothermal oxidation process at around 900°C. This rate decreasing is more obviously at a faster heating rate and keeps recovering to the theoretical value with the continuous oxidation [17]. Abuluwefa et al. agree with the method that scale separation causes the oxidation rate to decrease. The microstructure of the scale is observed by Abuluwefa et al and Figure 2-6 shows the separation of the scale.

Sachs and Tuck also finds that the recovery of the scale formation rate decreasing is related to the water concentration in the atmosphere [17]. For this phenomenon, Chen and Yuen did a series of experiments of the scale formation rate in a nitrogen-based atmosphere with 1% oxygen and different fractions of water vapor from 0 to 24.8% at 800°C [28]. They found that the scale also became detached from the steel substrate at such temperature lower than 900°C because of growth stress. And the influence of water vapor is attributed to two methods. The dissociation of

water generates hydrogen at the interface of the scale and steel, first method is that hydrogen is incorporated into the scale layer, and improves the plasticity of the scale. Sufficient plastic flow of the scale could prevent the detachment of the scale from the steel substrate. The other method is that some of the hydrogen stayed at the surface of the steel slab and helps transfer the ion from the steel to the scale to reduce the transfer rate reduction of the interface.
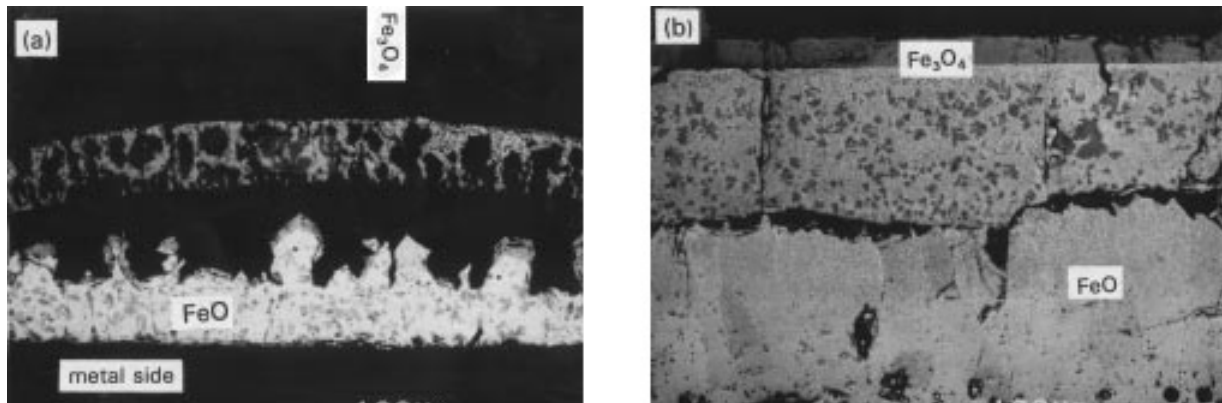
Figure 2-6 Scale microstructure of (a) laboratory experiments and (b) reheating in industrial furnace [21]

Another phenomenon is that, as shown in Figure 2-7, when the detachment happens, new scale may generate at the surface of the steel surface. In this situation, the scale formation rate changed to linear rate shortly and increase at this small area, until the newly formed scale fill the entire void or reach a specific thickness and changed back to the iron ion transfer controlled parabolic rate.

Figure 2-7 Scale separated surface

2.2.3 Scale composition and property

Scale mainly consists of wüstite, magnetite and hematite. The fractions of three ingredients change with the gas components, temperature and the composition of the steel. Since in the environment of reheating process, the formation of hematite is much less than the other two, the scale can be simplified considered as con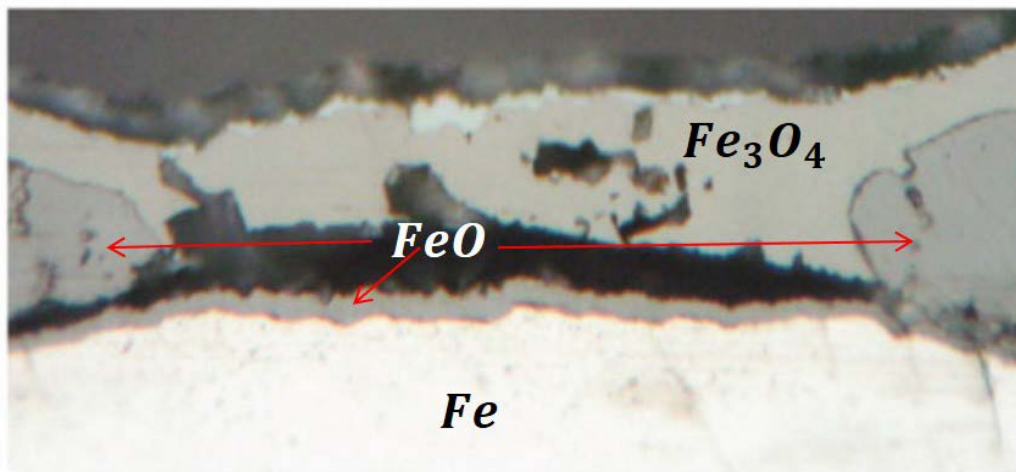sisting of wüstite and magnetite. Yurek et al. developed a two-phase layered scale formation method that can calculate the thickness of different components [29]. As shown in Figure 2-8, Me is the assumed pure metal, Me_vO and $Me_\delta O$ are two types of oxide of the Me, ζ and η are the thickness of two layers. P_{O_2} is the equilibrium partial pressure of the oxygen at the specific position.
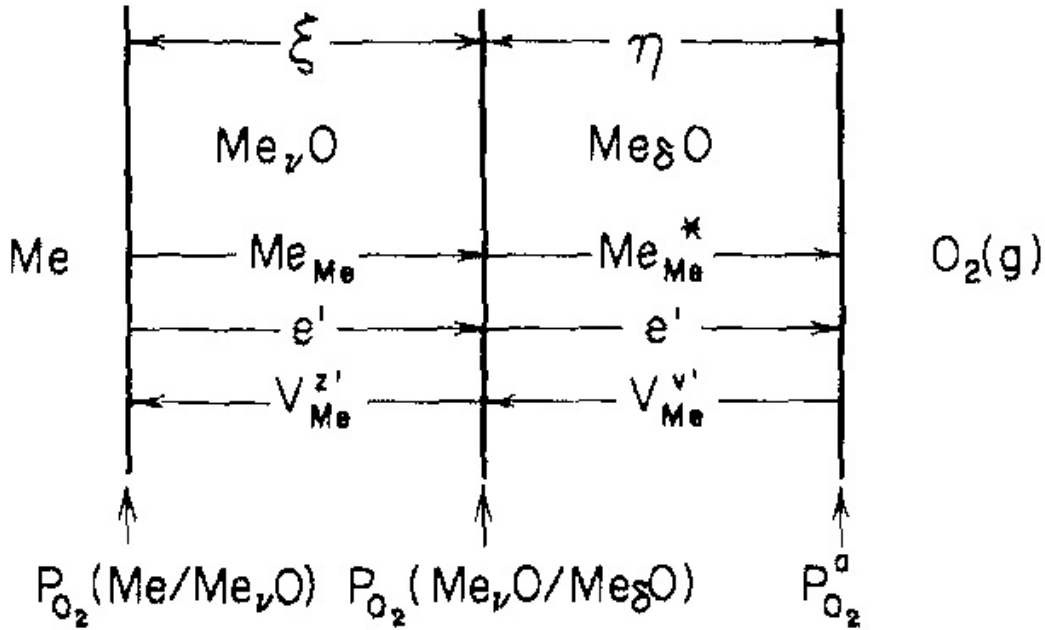
Figure 2-8 A model for the growth of a two-phase layered scale

According to the assumption of the model, the global reaction equation is:

$$(vw + \delta y)Me + \left(\frac{w+y}{2}\right)O_2 \rightarrow wMe_vO + yMe_\delta O \tag{2.9}$$
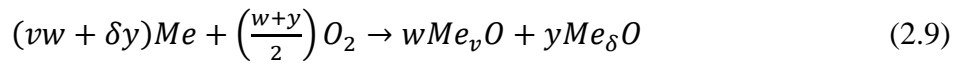
Using the diffusion controlled method to consider the formation rate of two oxide, which means the flux of the Me atom through the scale need to be equilibrium with the consumption of the oxidation. The global equation can be separated into two separate reactions:

$$(vw - \delta w)Me + wMe_\delta O \rightarrow wMe_vO \tag{2.10}$$
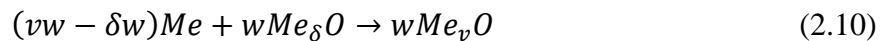
At the interface of Me_vO and $Me_\delta O$, and

$$(\delta w + \delta y)Me + \left(\frac{w+y}{2}\right) O_2 \rightarrow (w + y)Me_\delta O \tag{2.11}$$

At the surface of Me$_\delta$O layer. For the diffusion controlled scale formation, the parabolic rate constant of thickness K$_p$ represent the thickness change ability constant while all the transferred metal atom is reacted. At such situation, relationship between scale thickness x and K$_p$ is

$$dx/dt = K_p/x \tag{2.12}$$

So, for present method the equation changes into

$$d\zeta/dt = [wv/(vw + \delta y)]K_p(Me_v O)/\zeta \tag{2.13}$$

$$d\eta/dt = [\delta y/(\delta w + \delta y)]K_p(Me_\delta O)/\eta \tag{2.14}$$

$K_p(Me_v O)$ and $K_p(Me_\delta O)$ means K_p of the specific material.

Since a constant scale species fraction is assumed

$$\frac{d\zeta/dt}{d\eta/dt} = \frac{\zeta}{\eta} = \frac{wV_{Me_v O}}{vV_{Me_\delta O}} \tag{2.15}$$

$V_{Me_v O}$ and $V_{Me_\delta O}$ are the molar volume of two oxides in layers.

According to the atom transfer method,

$$K_p = \frac{1}{2}\int_{P'}^{P''} \frac{Z}{|Z_O|} D_{Me} \, d(lnP_{O_2}) \tag{2.16}$$

in which P' and P'' are the partial pressure of oxygen at the boundary on the oxygen side and on the pure metal side of the oxide layer, Z and Z_O are the valence of metal and oxygen and D_{Me} is the diffusion coefficient of Me in the oxide. For metal iron, the diffusion coefficient of iron in magnetite has been studied by Dieckmann and Schmalzried [30] and summarized as a function of temperature and oxygen partial pressure. Then the scale thickness ratio ζ/η then can be calculated by solving equations 2.13-2.16.

Garnaud and Rapp applied the above method on the steel oxidation [31], since solving functions is a complex process, an assumed scale thickness ratio of 0.95/0.05 is assumed, and the calculated value is $\eta/\zeta = 0.041$ at 1100°C, so the assumption that 4% of the scale is the magnetite is confirmed as acceptable, and it's also match the experimental result shown in Figure 2-9.
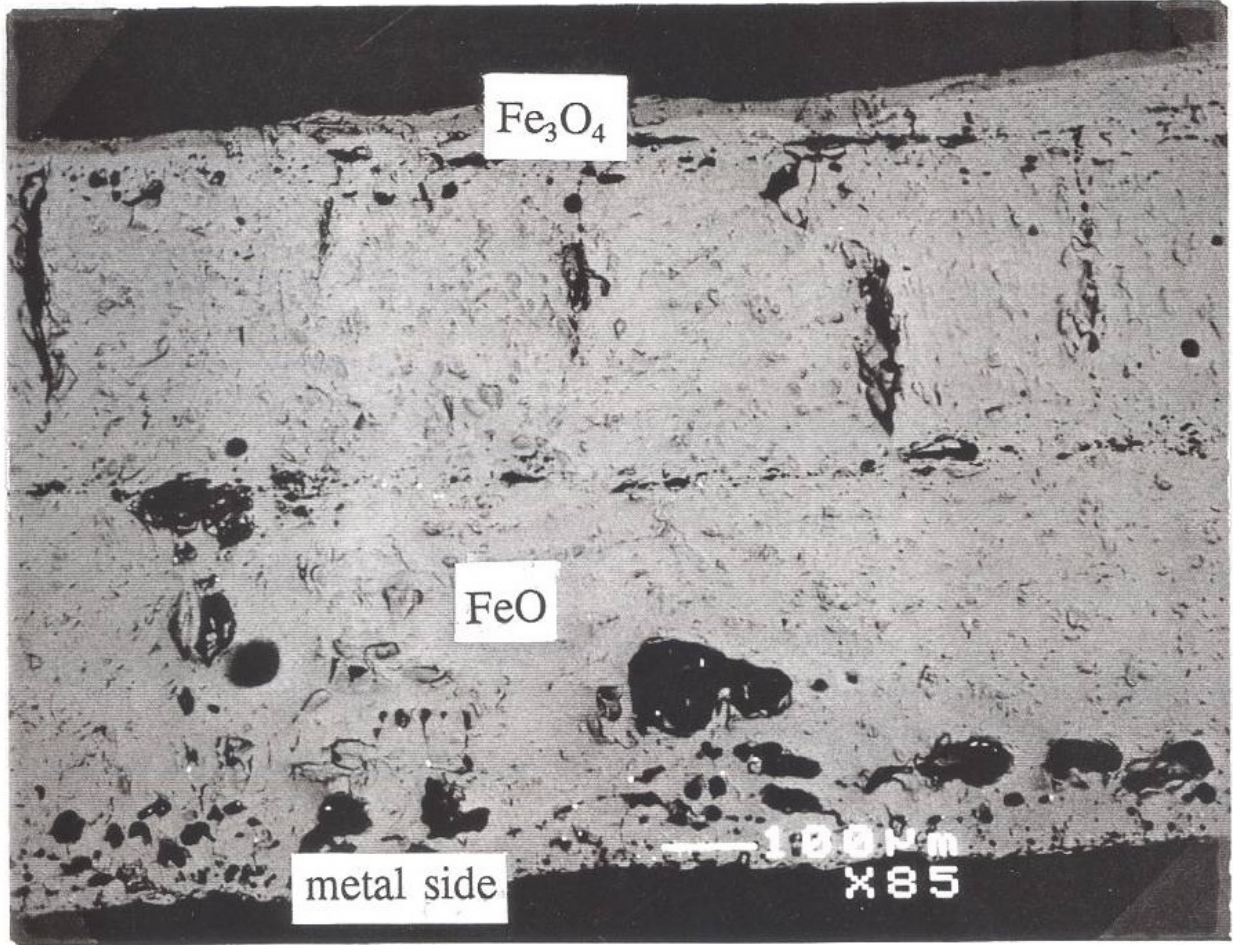
Figure 2-9 Scale structure after oxidation in the industrial reheat furnace [32]

Since the scale layer covered the surface of the slab, the heat transfer from the furnace to the slab needs to get through the scale layers, and the heat transfer property of the scale changes the heat transfer efficiency of the heating. Grønvold et al did a research of the property of wüstite and magnetite [33]. Thermodynamic properties of FeO, Fe_3O_4 and the process Fe_3O_4 transfer to FeO from 298 to 1250K are all obtained and listed in the research. The property of more oxides including Fe_2O_3 and $FeSiO_4$ are studied by Takeda et al [34]. A study of the influence of the oxide scale on heat transfer during reheating has been done by Wikström et al [35]. The heat transferred through the scale layer q in the research is calculated as:

$$q = k_0 \left(T_{scale}(t) - T_{steel}(t) \right)/d(t) \tag{2.17}$$

where k_0 is the thermal conductivity. It's the same with the general phase to phase heat transfer equation. In the research, it was found that around 1.1% of total energy consumption is absorbed

by the scale and the scale surface temperature is 50 to 200°C higher than the steel surface temperature. A theory of energy changing of the scale layer is also included in the research of Abuluwefa, Guthrie and Ajersch. The theory considered both the formation energy of the scale and convection, radiation heat transfer from gas. The equation of thermal conductivity calculation is also given in the literature.

3. CFD MODELS

The governing equations determine the solution of simulation through solving the conservation equation of momentum, mass and energy, along with scalar transport equation. ANSYS Fluent were used as simulation software. Several models are applied and their conservation equations are also need to be solved during the simulation.

3.1 Governing equations

Conservation of mass is the most basic criterion in a simulation, the mass conservation equation is:

$$\frac{\partial \rho}{\partial t} + \nabla \cdot (\rho \vec{v}) = 0 \tag{3.1}$$

where ρ is density, t refers to time and $\vec{v}$ is the velocity vector.

The conservation of momentum is solved by:

$$\frac{\partial}{\partial t}(\rho \vec{v}) + \nabla \cdot (\rho \vec{v} \vec{v}) = -\nabla p + \nabla \cdot (\bar{\bar{\tau}}) + \rho \vec{g} \tag{3.2}$$

where p is the static pressure, $\rho \vec{g}$ represent the gravity body fore and the stress factor $\bar{\bar{\tau}}$ is calculated by:

$$\bar{\bar{\tau}} = \mu[(\nabla \vec{v} + \nabla \vec{v}^T) - \frac{2}{3}\nabla \cdot \vec{v}I] \tag{3.3}$$

where μ is the molecular viscosity and I is the unit tensor.

The energy equation is solved in the following form:

$$\frac{\partial}{\partial t}(\rho E) + \nabla \cdot \left((\rho E + p)\vec{v}\right) = \nabla \cdot (k_{eff}\nabla T - \sum_j h_j \vec{J}_j + \left(\bar{\bar{\tau}}_{eff} \cdot \vec{v}\right)) + S_h \tag{3.4}$$

where k_{eff} is the effective thermal conductivity, $\bar{\bar{\tau}}_{eff}$ is the effective stress tensor, $\vec{J}_j$ is the diffusion flux of species j, S_h represents source terms including source term from the radiation model and heat source term from scale formation calculated before, h is the sensible enthalpy, and E is the total energy defined by:

$$E = h - \frac{p}{\rho} + \frac{v^2}{2} \tag{3.5}$$

For the non-premixed, non-adiabatic combustion model, the total enthalpy can be calculated from:

$$\frac{\partial}{\partial y}(\rho H) + \nabla \cdot (\rho H \vec{v}) = \nabla \cdot (\frac{k_t}{C_p} \nabla H) + S_h \tag{3.6}$$

where H is the summation of the product of mass fraction and enthalpy for each species. C_p is the specific heat with constant pressure.

The realizable k-ε turbulence model is chose as the turbulence model which can reach a balance between the computational cost and result accuracy. The transport equations for k and ε are:

$$\frac{\partial}{\partial t}(\rho k) + \frac{\partial}{\partial x_j}(\rho \varepsilon u_j) = \frac{\partial}{\partial x_j}\left[\left(\mu + \frac{\mu_t}{\sigma_k}\right)\frac{\partial k}{\partial x_j}\right] + G_k + G_b + \rho\varepsilon - Y_M \tag{3.7}$$

$$\frac{\partial}{\partial t}(\rho \varepsilon) + \frac{\partial}{\partial x_j}(\rho \varepsilon u_j) = \frac{\partial}{\partial x_j}\left[\left(\mu + \frac{\mu_t}{\sigma_\varepsilon}\right)\frac{\partial \varepsilon}{\partial x_j}\right] + \rho C_1 S_\varepsilon - \rho C_2\left(\frac{\varepsilon^2}{k+\sqrt{v\varepsilon}}\right) + C_{1\varepsilon}(\frac{\varepsilon}{k})C_{3\varepsilon}G_b \tag{3.8}$$

where $C_1 = \max\left[0.43, \frac{\eta}{\eta+5}\right], \eta = S\frac{k}{\varepsilon}, S = \sqrt{2S_{ij}S_{ij}}$, u is the velocity component, x is the direction component, μ is the molecular viscosity, and μ_t is the turbulent viscosity. G_k and G_b are the generation of turbulence kinetic energy from the mean velocity gradients and due to buoyancy respectively. Y_M represents the contribution of the fluctuating dilatation in compressible turbulence to the overall dissipation rate. $C_{1\varepsilon}, C_2, \sigma_k, \sigma_\varepsilon$ are four constants with value 1.44, 1.9, 1.0, 1.2.

3.2 Combustion and radiation model

The discrete ordinates (DO) radiation model is used for radiation calculation, the model solves the radiative transfer equation for a finite number of discrete solid angles, each associated with a vector direction $\vec{s}$ fixed in the global Cartesian system. The DO model consider the radiative transfer equation in the direction $\vec{s}$ as a field equation written as:

$$\nabla \cdot (I(\vec{r},\vec{s})\vec{s}) + (a + \sigma_s)I(\vec{r},\vec{s}) = an^2\frac{\sigma T^4}{\pi} + \frac{\sigma_s}{4\pi}\int_0^{4\pi} I(\vec{r},\vec{s}')\Phi(\vec{s},\vec{s}')d\Omega' \tag{3.9}$$

where $\vec{r}$ is the position vector, $\vec{s}'$ is the scattering direction vector, a is the absorption coefficient, σ_s is the scattering coefficient, I is the radiation intensity, σ is the Stefan-Boltzmann constant, Φ is the phase function and Ω' is the solid angle. The weighted-sum-of-gray-gases model (WSGGM) have been studied and have good result in literatures, the basic assumption of WSGGM is that the total emissivity over the distance S can be presented as

$$\varepsilon = \sum_{i=0}^I a_{\varepsilon,i}(T)(1 - e^{-K_i p S}) \tag{3.10}$$

where $a_{\varepsilon,i}$ is the emissivity weighting factor for the ith fictitious gray gas, the bracketed quantity is the ith fictitious gray gas emissivity, K_i is the absorption coefficient of the ith gray gas, p here is the sum of the partial pressures of all absorbing gases, and S is the path length. Comparing with the gray gas model with absorption coefficient a, a is estimated as

$$a = \frac{ln(1-\varepsilon)}{S} \tag{3.11}$$

To simplify the computation, a two-step methane combustion mechanism is used and volumetric species transport model is used to calculate species. The reactions of two-step methane combustion are:

$$2CH_4 + 3O_2 \rightarrow 2CO + 4H_2O \tag{3.12}$$
$$2CO + O_2 \rightarrow 2CO_2 \tag{3.13}$$

Species transport model predicts the local mass fraction of each species, Y_i, through the solution of a convection-diffusion equation for the ith species. This conservation equation takes the following general form:

$$\frac{\partial}{\partial t}(\rho Y_i) + \nabla \cdot (\rho \vec{v} Y_i) = -\nabla \cdot \vec{J}_i + R_i + S_i \tag{3.14}$$

where R_i is the net rate of production of species i by chemical reaction and S_i is the rate of creation by addition from the dispersed phase plus any user-defined sources.

3.3   Scale formation

According to the reviewed literatures, there are several different mechanisms of scale formation in different situations. Considering the actual influence of each mechanism on the reheating process, cost of computing and computability of the theory, using some simplified assumption instead of a whole mechanism is needed. The main mechanism is the reaction with oxygen which is also the main purpose of this thesis research. Oxidization caused by CO_2 and H_2O happens most situations and has a large influence on scale formation rate at the initial stage of oxidation, so it also needs to be considered. The scale separation around and below 900°C is an important phenomenon and have a large influence on the scale formation rate, but since the scale separation is kind of random and incomputable using present theory, the influence of detachment of scale need to be ignored and accuracy of the method will be lower below 950°C.

For the alloy elements, the main material studied in reviewed literature is low alloy mild steel with around 0.05% carbon. According to Abuluwefa [19], carbon has been shown to decrease the scaling rate of steel because of reducing the ion diffusion and reacting with oxygen or metal oxide. So the product need to be assumed as low carbon steel, for other steel, the accuracy of simulation will decrease. For other alloy elements, their effect is complex. Manganese does not contribute to any major effect on the oxidation of steel. Copper and nickel tend to concentrate at the steel/oxide interface which lowers the oxidation rate, on the other hand, nickel alloy has the tendency to increase scale adhesion to the substrate, which may increase the scale formation rate below 950°C. The protective layer of Cr_2O_3 or Al_2O_3 can isolate the metal from gas and reduce the oxidation rate. And silicon can react with oxygen, the product, SiO_2, can form fayalite, $2FeO·SiO_2$, which has a melting point of 1171°C. The molten fayalite can accelerate the ion diffusion and then increase the oxidation rate. Since most of the research is based on low alloy steel, the high alloying element concentration will influence the accuracy of the result.
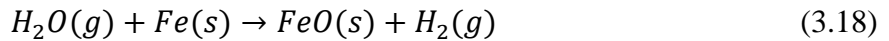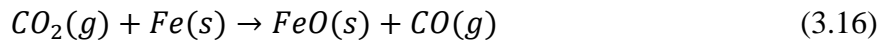
Since the composition of the scale will not have large changes during reheating process, and the mechanism of scale component calculation is complex, a volume fraction of 95:4:1 for $FeO:Fe_3O_4:Fe_2O_3$ is assumed [38].

3.3.1 Calculation of scale formation

Thermodynamic study of a system of a metal undergoing oxidation can answer many potent questions. The first is whether the reaction can happen or not. Three oxidizer is considered in the method, considering the FeO as the product, the oxidation reaction with O_2 is:

$$O_2(g) + 2Fe(s) \rightarrow 2FeO(s) \tag{3.15}$$

Since gas phase only exist in reactant side, oxygen can be fully reacted with enough iron. As for carbon dioxide and water, related reactions are:

$$CO_2(g) + Fe(s) \rightarrow FeO(s) + CO(g) \tag{3.16}$$

$$2CO + O_2 \rightarrow 2CO_2 \tag{3.17}$$

$$H_2O(g) + Fe(s) \rightarrow FeO(s) + H_2(g) \tag{3.18}$$

$$2H_2 + O_2 \rightarrow 2H_2O \tag{3.19}$$

Since O_2, CO, CO_2, H_2O and H_2 are all in the atmosphere, equilibrium of these gases need to be reach. The equilibrium constant K can be calculated by:

$$lnK = -\frac{\Delta G^\circ}{RT} \qquad (3.20)$$

For reaction (3.17) and (3.19), standard Gibbs free energy changing $\Delta G^\circ = -513.58\ kJ/mol$ and $-457.42\ kJ/mol$, at 1100°C equilibrium constant $K = 3.446\text{x}10^{19}$ and $2.517\text{x}10^{17}$. Since the equilibrium constant of this two reaction is large, it can be considered that when oxygen exist in the gas phase, hydrogen and carbon monoxide cannot be formed, which means reaction (3.16) and (3.18) won't happen when ion diffusion controlled the oxidation and oxygen cannot be fully reacted.

So the full oxidation process is divided into two parts, the initial linear part, controlled by oxidants, follow the equation:

$$W/A = k_l t \qquad (3.21)$$

And the ion diffusion controlled parabolic part, follow the equation:

$$(W/A)^2 = k_p t \qquad (3.22)$$

W is the weight gained from atomic oxygen in oxides with unit g, A is the area of the reaction surface with unit cm^2, t is the slab residence time (unit s) and k_l and k_p are linear and parabolic oxidation rate constants. And it can be derived that

$$\frac{d(W/A)}{dt} = k_l \qquad (3.23)$$

$$\frac{d(W/A)}{dt} = \frac{k_p}{2(W/A)} \qquad (3.24)$$

Above equations can be used for calculate the linear and parabolic scale formation rate.

The rate constant k_l and k_p are based on different properties. As mentioned before, linear rate constant is influenced by three oxidant, oxygen, carbon dioxide and water vapor, so the linear rate constant is the summation of the rate of all the oxidizing species:

$$k_l = k_{l,CO_2} + k_{l,H_2O} + k_{l,O_2} \qquad (3.25)$$

where k_{l,CO_2}, k_{l,H_2O} and k_{l,O_2} are the linear rate constant of CO_2, H_2O and O2. The scale formation rate formed by CO_2 and H_2O are mainly controlled by the reaction related to the surface reaction rate constant, oxygen activity of scale and partial pressure of the gas. An equation is developed by Pettit and Wagner to calculate the linear oxidation rate of CO_2 [14]:

$$k_{l,CO_2} = M_O k_{CO_2} a_O^{*-\frac{2}{3}} (1 - \frac{a_O^*}{a_O'}) P_{CO_2} \qquad (3.26)$$

where M_O is the molar weight of the oxygen atom, k_{CO_2} is a rate constant of phase boundary reaction, a_O is the oxygen activity of wüstite in equilibrium with iron (a_O^*) and in equilibrium with the gas phase (a_O'), P_{CO_2} is the partial pressure of CO_2 in gas. The rate constant of reaction k_{CO_2} represent the relationship between reactants and the reaction rate and can be given in the form of the Arrhenius equation:

$$k_{CO_2} = ce^{-E_{CO_2}/RT} \tag{3.27}$$

where c is a constant, R is the gas constant, T is the gas temperature and E_{CO_2} is the heat of activation of reaction (3.16). The value of E_{CO_2} calculated from the experimental data by Pettit and Wagner is 51 kcal [14] which is similar to the result 52 kcal of Turkdogan et al. [15], so the experimental result of Pettit and Wagner is used, which is:

$$c = 101.8 \tag{3.28}$$

$$E_{CO_2} = 51 \, kcal = 213384 \, J \tag{3.29}$$

The oxygen activity of reaction (3.16) can be calculated by equation:

$$a_O = P_{CO_2}/P_{CO} \tag{3.30}$$

One prediction base on the experimental data (Table 3-1) from Darken and Gurry is that [13]:

Table 3-1 Equilibrium gas constant at boundaries

T,°C	Iron—Wüstite (a_O^*)		Wüstite—Magnetite (a_O')	
	P_{CO_2}/P_{CO}	P_{H_2O}/P_{H_2}	P_{CO_2}/P_{CO}	P_{H_2O}/P_{H_2}
1100	0.355	0.738	6.12	12.7
1200	0.322	0.802	8.02	20.0
1300	0.297	0.861	10.79	31.3
1350	0.285	0.888		
1400			15.03	49.9

$$a_O^* = 0.0991e^{0.003T} \tag{3.31}$$

$$a_O' = 1.173e^{-0.0009T} \tag{3.32}$$

The same method is applied on the water vapor, so equation (3.26, 3.27), can also be used to calculate the linear scale formation rate of water vapor, but since the reactant is not the same, several constant and parameters need to be changed. Yin et al [25] have a same result with Turkdogan et al [15] that the activation heat of reaction (Eq. 3.18) is around 80,290 J (19.2 kcal), and base on Yin's equation, parameters are calculated as:

$$c = 0.002 \tag{3.33}$$

$$E_{H_2O} = 19.2 \ kcal = 80333 \ J \tag{3.34}$$

$$a_O^* = 0.02441e^{0.0046T} \tag{3.35}$$

$$a_O' = 0.2677e^{0.0007T} \tag{3.36}$$

As for the k_{l,O_2}, study of Deich and Oeters suggests that the reaction rate is mainly controlled by the transfer rate of oxygen from gas bulk to metal surface, and mainly related to gas flow property and concentration distribution of the oxygen [18].

$$k_{l,O_2} = 2M_O\beta(C_{O_2,gas} - C_{O_2,surface}) \tag{3.37}$$

β is a factor of mass transfer coefficient of gas flow, C_{O_2} is the oxygen concentration in gas $(C_{O_2,gas})$ or at slab surface $(C_{O_2,surface})$. According to the previous calculation, when the linear rate constant is used, oxygen at surface need to be zero or nearly zero, so $C_{O_2,surface}$ can be assumed to be zero. The factor β can be calculated by equation:

$$\beta = \frac{2}{3}\sqrt{\frac{D_{O_2}u}{l}} \ \sqrt[6]{\frac{D_{O_2}}{v}} \tag{3.38}$$

Where D_{O_2} is the diffusion coefficient of oxygen in furnace gas, u is the gas velocity, l is the characteristic length of the slab which is the length along the gas flow or slab moving direction and v is the kinematic viscosity. Viscosity normally can be measured or calculated using mixture property in experimental environment or calculated by CFD software when using CFD, so the calculation of viscosity will not be discussed further here. For D_{O_2}, data measured by Deich and Oeters is used (Table 3-2).

Table 3-2 Diffusion coefficient of oxygen

Temperature(°C)	$D_{O_2-N_2}$ (cm^2/s)	$D_{O_2-N_2-CO_2}$ (cm^2/s)
800	1.74	1.56
900	2.01	1.80
1000	2.29	2.06
1100	2.59	2.32

And a trend line equation of the data is :

$$D_{O_2} = 0.00283T - 1.304 \tag{3.39}$$

Since most of the consistent gas inside the furnace gas is still nitrogen, the oxygen diffusion coefficient is simplified use the value in nitrogen, for the oxygen enrichment combustion with less

nitrogen attend, especially pure oxygen-fuel combustion, the diffusion coefficient might be smaller and can use below equation instead:

$$D_{O_2} = 0.00254T - 1.172 \tag{3.40}$$

The factor β can be also expressed as a function of dimensionless numbers $Re(ul/v)$, Reynold number, and $Sc(v/D_{O_2})$, Schmidt number, as follows:

$$\beta = \frac{2}{3}\frac{D_{O_2}}{l}\sqrt{Re}\sqrt[3]{Sc} \tag{3.41}$$

The linear rate constant is sensitive to the environment flow field property, so the edge effect and the flow velocity differences can highly influence the result. It's suggest that for the sample with shortest edge length less than 2cm, a factor of 5/3 need to by multiplied to total linear rate to fix the influence of edge effect, and for flow with large velocity change along the slab surface, a correction factor might be needed for the linear rate constant of oxygen (k_{l,O_2}).[22]

The parabolic rate is controlled by the diffusion of the iron ion. The formula of the rate constant was derived based on phase equilibria of ion and scale properties:

$$k_p = 6\frac{\rho_{FeO}^2 M_O^2}{M_{FeO}^2}D_{Fe^{2+}}^*(\gamma_{FeO/Fe_3O_4} - \gamma_{Fe/FeO}) \tag{3.42}$$

M_{FeO} is molecular weight of wüstite, ρ_{FeO} is density of wüstite, $D_{Fe^{2+}}^*$ is iron self-diffusion coefficient and γ signifies the iron ion vacancy concentration at boundaries of wüstite layer. Abuluwefa used the equation below to calculate the iron self-diffusion coefficient [27], where the unit of energy is J and R=8.314.

$$D_{Fe^{2+}}^* = 0.118e^{-124300/RT} \tag{3.43}$$

Deich and Oeters used an equation with calorie as the unit of energy and R=1.987 [18].

$$D_{Fe^{2+}}^* = 0.045e^{-27800/RT} \tag{3.44}$$

Comparing with the experimental value, as shown in Figure 3-1, equation (3.43) matches the experimental value well below 1000°C, and at temperature higher than 1050°C, equation (3.44) matches better. So a combined equation is used, which use the more accurate parts of two equations at specific temperature range and add a transition curve between 1000 and 1050°C.
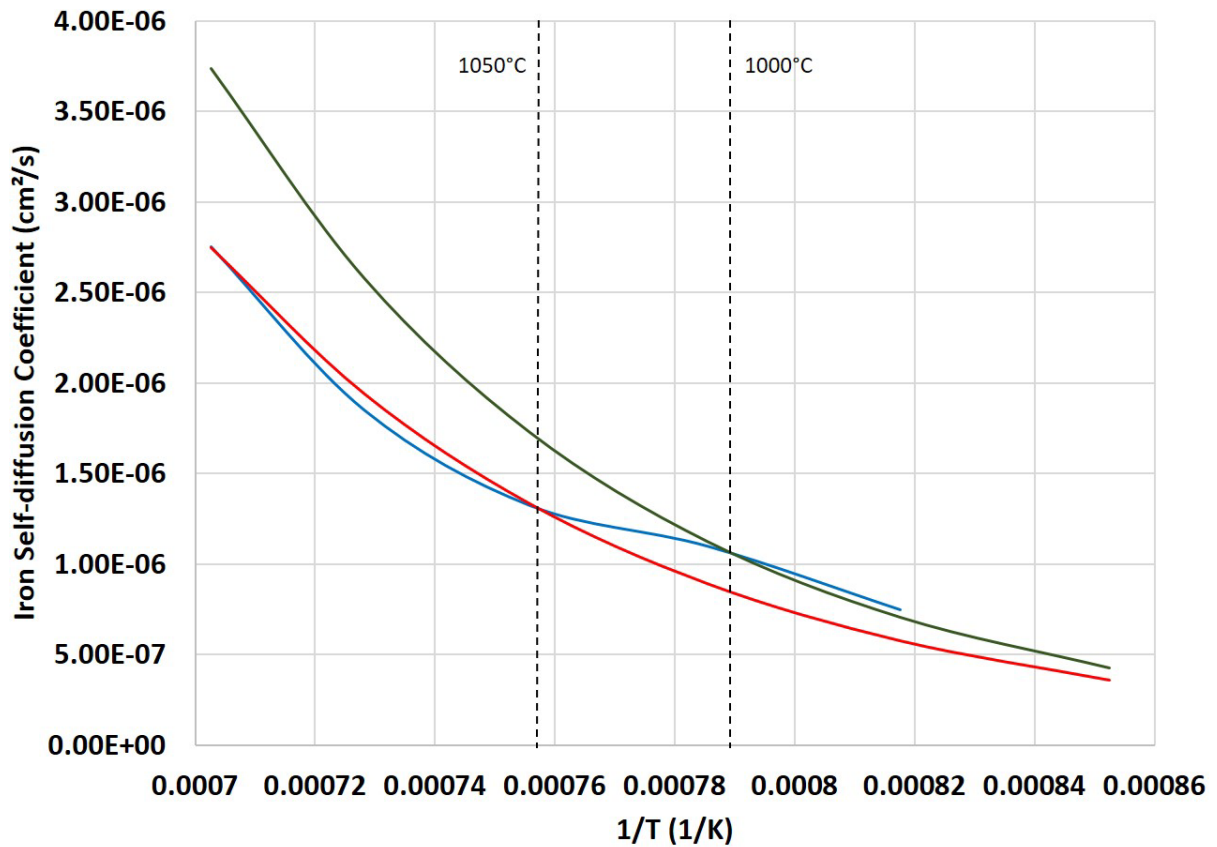
Figure 3-1 Iron self-diffusion coefficient equations compare with experimental value

Deich and Oeters also provided tabulated data for iron ion vacancy concentrations at boundaries of wüstite (Table 3-3).

Table 3-3 Iron ion vacancy concentration

Temperature(°C)	γ_{FeO/Fe_3O_4}	$\gamma_{Fe/FeO}$
800	0.108	0.053
900	0.117	0.050
1000	0.125	0.049
1100	0.130	0.047

The concentration values of two boundaries can be summarized as below equation:

$$\gamma_{FeO/Fe_3O_4} = -1 \times 10^{-7}T^2 + 2.64 \times 10^{-4}T - 0.0393 \qquad (3.45)$$

$$\gamma_{Fe/FeO} = 2.5 \times 10^{-8}T^2 - 6.65 \times 10^{-5}T + 0.0901 \qquad (3.46)$$

In two equations above the unit of the temperature T is °C.

41

Formulas above can deduce rate constants that describe the weight gain per unit area. To convert the rate of W/A to rate of thickness growth x, a conversion factor has been derived as:

$$W/A = x \sum_{i=1}^{n} w_i \rho_i r_i \tag{3.47}$$

where w is the weight fraction of oxygen element in the oxide, ρ is the density of the oxide and r is the thickness fraction of the oxide in scale. Properties of three considered oxides are listed in Table 3-4. Due to the high thickness fraction of wüstite, temperature dependent property value are used for it to improve accuracy.

Table 3-4 Physical properties of the iron oxides

Iron Oxide	Weight fraction of O	Density (g/cm^3)	Thickness fraction
Wüstite	16/(16+(-5e^{-5}T+0.9816)*55.845)	(-0.0001T)+5.7467	95%
Magnetite	27.64%	5.18	4%
Hematite	30.06%	5.255	1%

Since the scale formation rate is separated into two parts, a transition thickness is needed to judge whether linear or parabolic rate scale formation is followed. According to the controlling factor in the present method, the maximum possible reaction rate of oxidant is controlled by both surface reaction rate and gas transfer rate and the maximum possible reaction rate of iron is controlled by iron ion transfer rate. Since iron and oxidant are the reactants of oxidation, so the oxidation reaction rate is controlled by the slower one of two rates. So the transition of oxidation rate from linear to parabolic happens when two rates reach the same value. Thus

$$\frac{d(W/A)}{dt} = \frac{k_p}{(W/A)} = k_l \tag{3.48}$$

Define $\sum_{i=1}^{n} w_i \rho_i r_i$ as the oxygen density in the scale $\rho_{O_2,scale}$, from equation (3.47) and (3.48):

$$x = k_p / (\rho_{O_2,scale} k_l) \tag{3.49}$$

3.3.2 Calculation of scale heat generation

Since the reaction rate of oxidation is highly dependent to the temperature of the reaction surface, the heat of formation of scale can obviously raise the surface temperature. So the heat of scale formation is needed to be considered. The heat released from the reaction equals the difference of enthalpy of the reactants and the products. Since only oxygen attend the reaction in parabolic rate oxidation and parabolic part normally takes most of the time of the oxidation, to simplify the calculation, reactants are assumed to be only oxygen and iron. The global reaction of simplified scale formation is:

$$0.57O_2 + 1.09Fe \rightarrow 0.95FeO + 0.04Fe_3O_4 + 0.01Fe_2O_3 \tag{3.50}$$
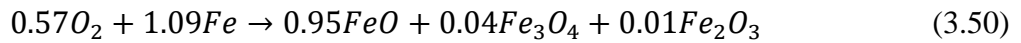
General formula of formation heat H (kJ/mol) is shown as below:

$$H = AT + BT^2/2 + CT^3/3 + DT^4/4 - E/T + F \tag{3.51}$$

A, B, C, D, E, F here are constants, the unit of T is 10^3K, for all the species attend the reaction, constants are shown in Table 3-2.

Table 3-5 Thermodynamic constants [39]

	A	B	C	D	E	F
O_2	30.03	8.77	-3.99	0.79	-0.74	-11.32
Fe	-776.74	919.4	-383.72	57.08	242.14	697.62
FeO	45.75	18.78	-5.95	0.85	-0.08	-286.74
Fe_3O_4	200.83	0	0	0	0	-1174.14
Fe_2O_3	110.93	32.05	-9.19	0.9	5.43	-843.15

From reaction (3.50), the reaction heat per molar oxygen atom ΔH_O and heat per unit area ($\Delta H/A$) can be deduced:

$$\Delta H_O = \frac{0.57H_{O_2} + 1.09H_{Fe} - (0.95H_{FeO} + 0.04H_{Fe_3O_4} + 0.01H_{Fe_2O_3})}{2 \times 0.57} \tag{3.52}$$

$$(\Delta H/A) = \Delta H_O \times (W/A)/16 \tag{3.53}$$

($\Delta H/A$) then can be used in CFD as a heat source term to simulate the heat of the reaction, this will be mentioned later.

43

3.3.3 Thermodynamic characteristic change of material

One of the main influence of scale layer is that the heat transfer rate from furnace to the slab is reduced because of the lower heat transfer coefficient of the scale layer. Consider the scale layer and a thin iron layer as the surface area of the slab, the assumed simplified structure is shown in Figure 3-2.
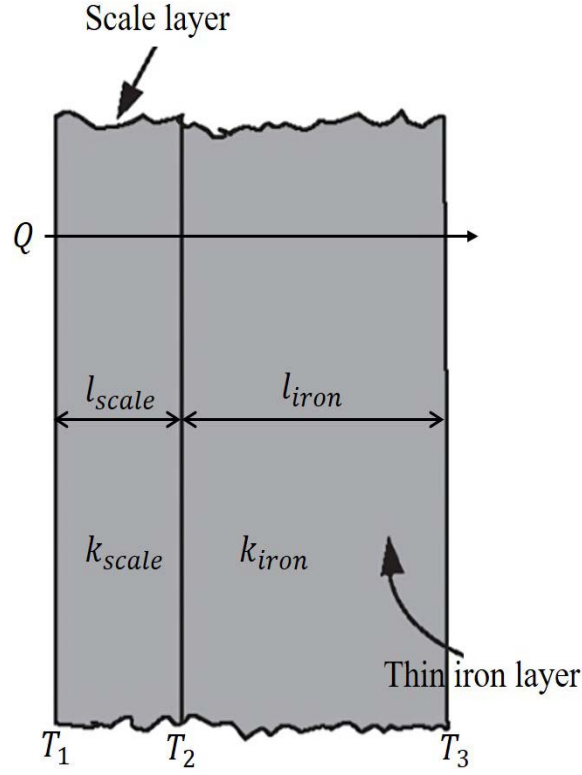

Figure 3-2 Model of heat transfer coefficient

In the figure, k is the thermal conductivity, l is the depth of the layer, T is the temperature of the surface or interface and Q is the transferred heat flux. According to the basic definition of the thermal conductivity, the average thermal conductivity of whole two layers k_{layer} can be formulated as:

$$Q = \frac{k_{scale}(T_1 - T_2)}{l_{scale}} = \frac{k_{iron}(T_2 - T_3)}{l_{iron}} = \frac{k_{layer}(T_1 - T_3)}{l_{scale} + l_{iron}} \tag{3.54}$$

Bring in $[(T_1 - T_2) + (T_2 - T_3)]/Q = (T_1 - T_3)/Q$

$$\frac{l_{scale} + l_{iron}}{k_{layer}} = \frac{l_{scale}}{k_{scale}} + \frac{l_{iron}}{k_{iron}} \tag{3.55}$$

$$k_{layer} = (l_{scale} + l_{iron})/(\frac{l_{scale}}{k_{scale}} + \frac{l_{iron}}{k_{iron}}) \tag{3.56}$$

And thermal conductivity of wüstite have been expressed as [40]:

$$k_{wüstite} = 1/(-1.047 \times 10^{-4}T + 0.3926) \tag{3.57}$$

Since the wüstite thickness fraction is much larger than other two oxide, to simplify the computation, $k_{scale} = k_{wüstite}$ can be assumed, then thermal conductivity of the slab surface area can be calculated by equation (3.56).

4. MODEL VALIDATION

Validation of the scale formation model needs to compare the simulation result with the experimental value in the same condition. The model was used to numerically replicate the experimental works done by Abuluwefa et al [27][20] and Deich and Oeters [18], in which tubular vertical furnaces were used (as shown in Figure 4-1) . Abuluwefa et al studied low carbon steel oxidation in different atmospheres and temperatures, and he also did several experimental studies of non-isothermal environment scale formation. Deich and Oeters conducted experiment studies of scale forming in a high carbon dioxide atmosphere. Both two groups of researchers provided detailed important conditions so that CFD cases can be built.
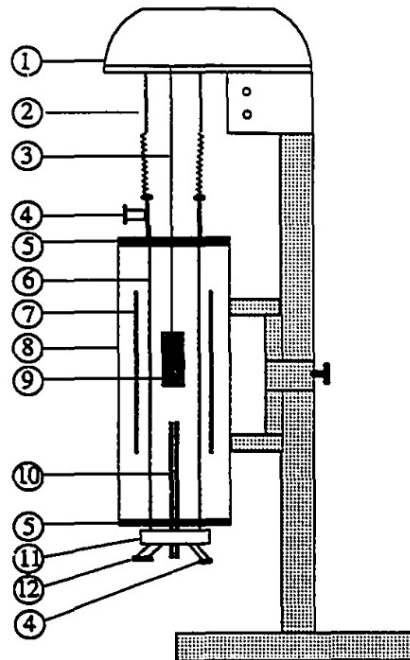
① High sensitivity microbalance.　⑦ Tungsten heating element.
② Flexible sealing tube.　⑧ Cylindrical pyrex-glass chamber.
③ Platinum suspension wire.　⑨ Test sample.
④ Gas inlet - outlet ports　⑩ Control thremocouples.
⑤ Water cooling flanges.　⑪ End flange equiped with view window.
⑥ Pure alumina furnace tube.　⑫ Connection port for vacuum pump.

Figure 4-1 Tubular vertical furnace

4.1   Geometry and mesh

The experimental device of studies are both tubular vertical furnaces. The experimental gas is injected into the furnace tube, goes through the surface of the sample, then exhausts through the outlet. Tube temperature is controlled by both cooling water and inlet gas temperature. The weight gained by scale formation is monitored continuously by the microbalance. In the study by Abuluwefa, the alumina reaction tube diameter is 14mm, length is 145mm, and the dimensions of steel samples are $18 \times 8 \times 8$mm. Deich and Oeters used a much larger furnace and sample, the furnace tube diameter is 50mm, and the size of the steel sample is $40 \times 40 \times 5$mm. In both two studies, the steel used is low carbon steel with 0.04% weight percent carbon.

The geometry and mesh used for validation are shown in Figure 4-2, to reduce the unnecessary cost of simulation, components that do not directly influence gas flow are not included in the mesh, and the flow field is simplified as flow from top to the bottom.
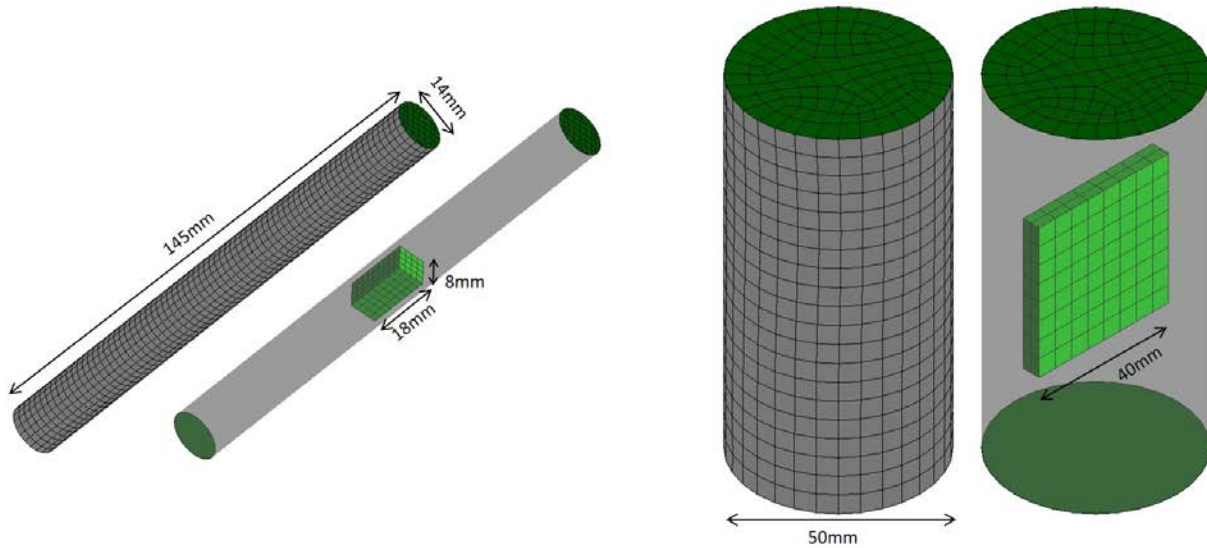

Figure 4-2 Validation case mesh of studies of Abuluwefa et al (left) and Deich and Oeters (right)

4.2   Boundary condition

In Abuluwefa's study, one of the gas he used to simulate the furnace gas is consist of 1% oxygen, 10% carbon dioxide, 3% water vapor and 86% nitrogen, so this is also used as the components of inlet species of corresponded case. The velocity of inlet gas is 11cm/s to ensure a sufficient gas supply for the process. A group of studies with different inlet temperatures have

been done to validate with Abuluwefa's study, inlet and furnace wall temperature settings are shown in Table 4-1. As for case for study of Deich and Oeters, the temperature is chosen to be 1100°C, inlet gas velocity is 20cm/s, the gas component changes in different cases, in both of three cases, 21% of carbon dioxide isn't changed, and oxygen and nitrogen fraction are shown in Table 4-1.

Table 4-1 Boundary condition of validation cases

Case#	Abuluwefa study case	Case#	Deich and Oeters study case	
	Temperature (°C)		Oxygen mole fraction	Nitrogen mole fraction
1	1050	**4**	1%	78%
2	1100	**5**	2%	77%
3	1150	**6**	3%	76%

4.3   Validation result

For the case of Abuluwefa's study, all the simulate cases show good correlation between simulation and experimental result, the average error between results are 0.9% to 2.8%, maximum weight error of three cases are 1.04, 1.31 and 1.84 mg/cm^2. Results are shown in Figure 4-3, where C represents degree Celsius and the simulation result is marked as simulated and the experimental result do not have such mark.
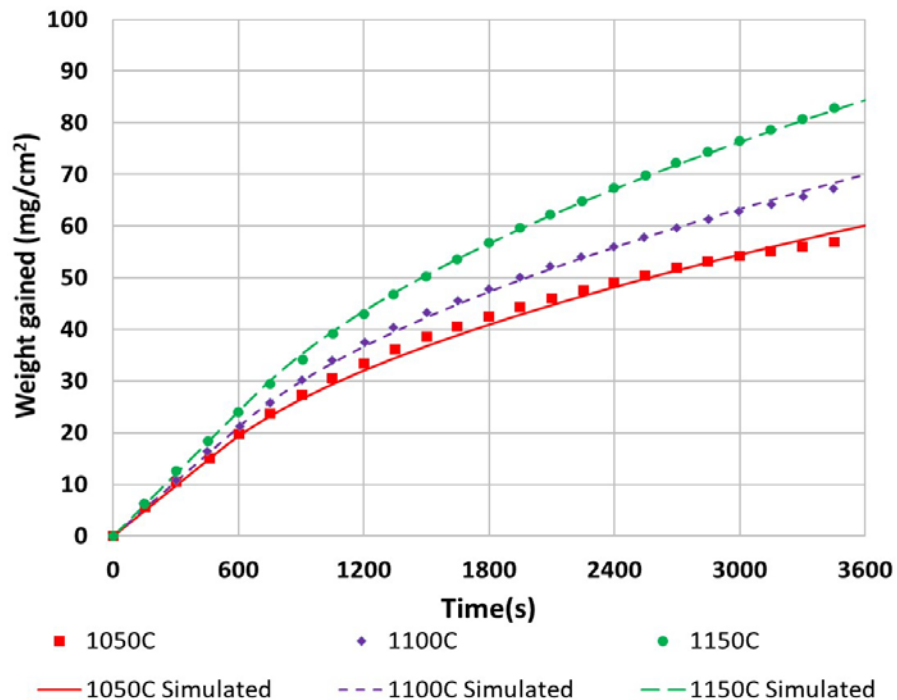

Figure 4-3 Validation result with Abuluwefa's study

The error of case 4, 5 and 6 is a little bit larger, the average error is 7.3%, maximum weight error is 6.1 mg/cm^2. As shown in the Figure 4-4, the simulation result of case 6 cannot matches the experimental data very well since it's not follow the linear rule nor parabolic rule, but since the trend is correct and the final result at 3500 seconds is quite similar, it is still acceptable.
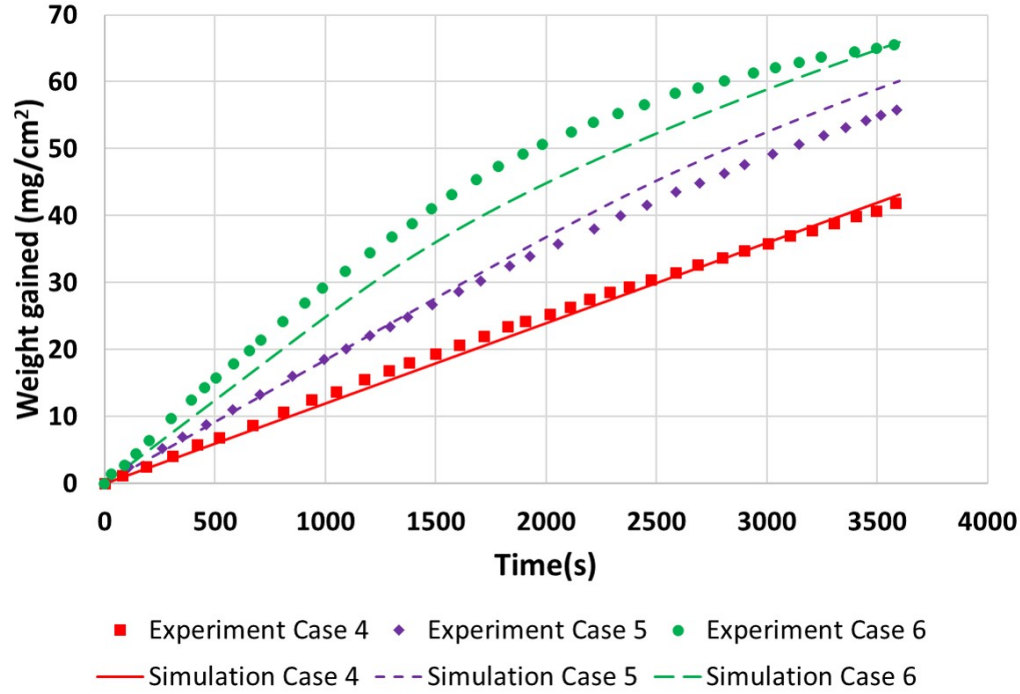

Figure 4-4 Validation result with Deich and Oeters's study

As mentioned before, considering the cost of the simulation, a steady-state furnace case is always used to compute the combustion and flow field in the reheating furnace simulation, so method application on the steady-state case is also need to be accomplished and validated. The validation of steady-state case is also base on the study of Abuluwefa, the oxidation time is same with the transient case, 3600 seconds, the movement direction of the material is assumed as from top, gas inlet direction to the bottom, gas outlet, and the moving distance in 3600s is from the solid zone top to the solid zone bottom, 18cm in total. The solid zone in case is divided into 9 layers of cells along the movement direction, so only 9 data points can be used in steady-state case. The result is shown in Figure 4-5, the error of result of three temperatures are in the range of 1.5% to 5.4%, maximum weight different with experimental value is 4.03 mg/cm^2.
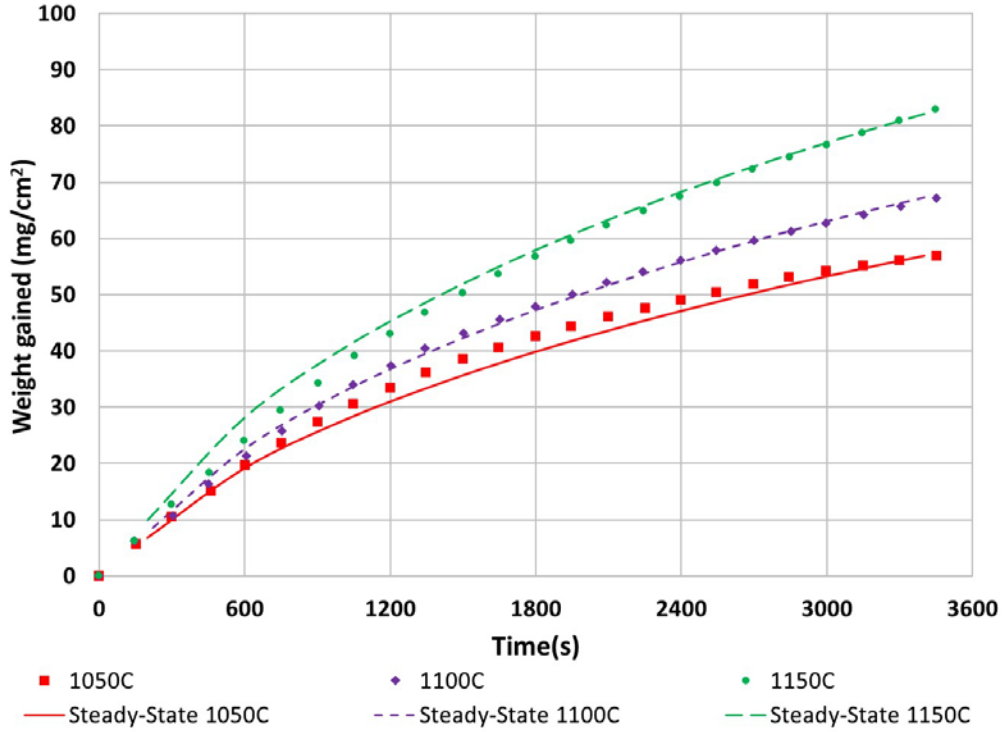
Figure 4-5 Validation of steady-state cases

The error of the steady-state case simulate result is larger than the error of transient case, the lack of data point is one of the main reason. For the larger case that separate slab surface plane into more columns of cells, the accuracy can be improved.

A calculator is developed base on the steady-state case, by using several types of flow field and material surface characteristic data at different times, the calculator can compute the scale thickness and mass during the oxidation. The calculator is shown in Figure 4-6. Since in the calculator, time can also be defined by coordinate and velocity, so a series data on one line can also be used to calculate the scale formation of a point move through the line. A validation using 11 data points is shown in Figure 4-7. If including the first point at 200 seconds, since the experimental value is small, the percentage error is quite large at the point, and the average error of three cases are 8.5%, 9.3% and 8.9%, it's a little bit larger. If the first point is ignored, the percentage error of three cases are 3.4%, 4.5% and 4.1%, and maximum weight differences are 2.08, 3.35 and $4.57 mg/cm^2$, which is acceptable.
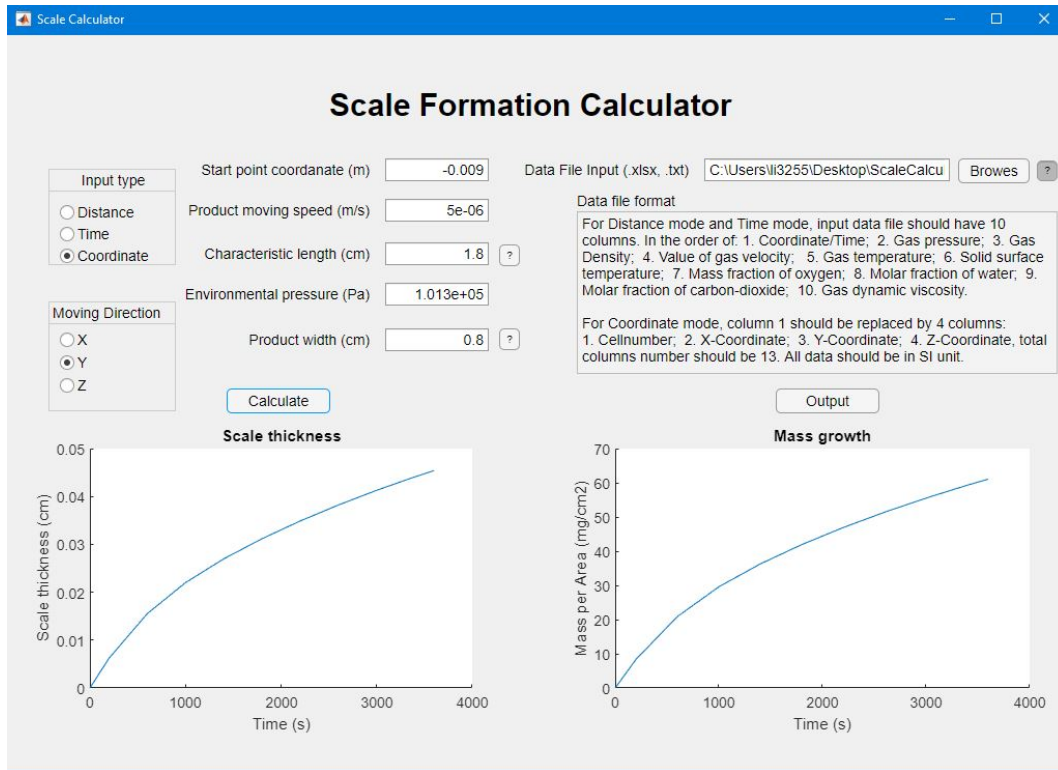
Figure 4-6 Scale Formation Calculator

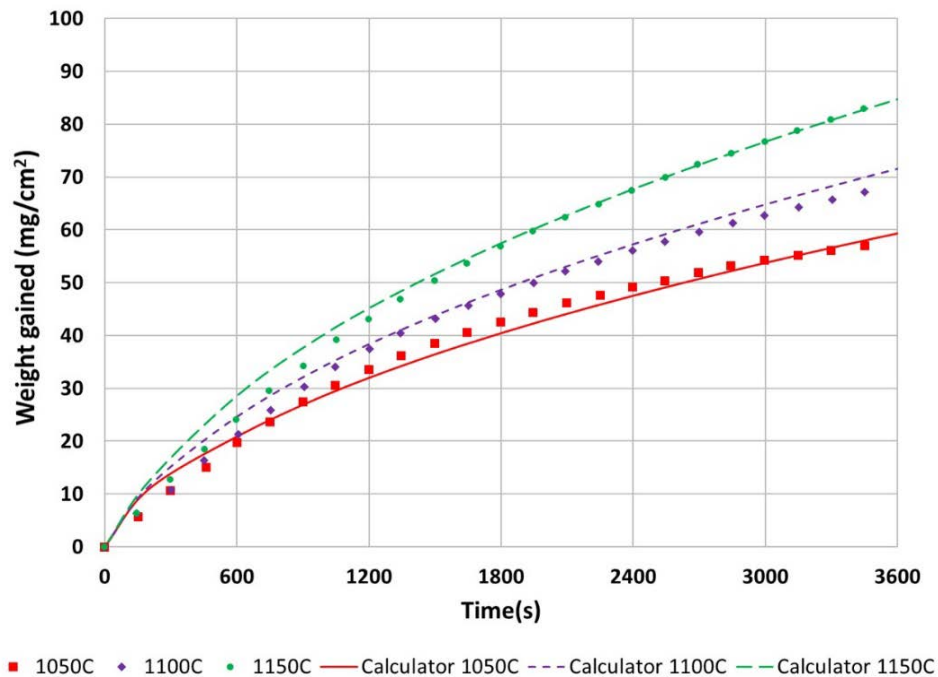

Figure 4-7 Validation of calculator

5. RESULT AND DISCUSSION

In present days, because of both the cost of the fuel and the requirement of the environment protection, more and more different types of fuel and oxidizer consistent are being considered using in reheating furnace. Oxygen enrichment using excess pure oxygen as oxidant instead of air have been considered for several years [11] and changing fuel from methane to other fuel like hydrogen is also not impossible. For all these possibilities, the heat transferred to the slab need to be same with the original furnace, since 95% of the heat transferred to the slab through radiation, the flame temperature and reaction heat need to be controlled to similar to normal fuel-air combustion. But since convection heat transfer is much less, the total gas flow rate and gas temperature may changes a lot in this situation, so a group of parametric study is done to study the influence of gas flow rate changing of the furnace to the scale formation. To simplify the calculation, the combustion heat is assumed to not change with the flow rate changing.

5.1 Baseline result

The case used is a steady-state walking beam reheating furnace case with mapped slab surface temperature, which means the slab surface temperature won't change during the computing. The whole reheating process is set to 138 minutes. The data of the centerline of slabs is used to represent the property of the slab surface, the used temperature curves are shown in Figure 5-1.

Except for the temperature, since the gas velocity, density, component and the turbulence flow of gas can also influence the scale formation, so data of these parameters are also shown in Figure 5-2. Pressure and viscosity are also important parameters but since in this simulation, pressure near the slab surface are nearly a constant of 1atm, viscosity is a constant 1.72e-5, they aren't shown in the picture.

As shown in the figure, the slab surface temperature is assumed to be heated at a constant rate, and because of gaps between slabs, some sudden drops or raise appears in the curves. Although it is a simplified furnace case, the data is enough for doing the scale formation calculation. For the baseline case, the computed mass of scale formation is shown in. Figure 5-3
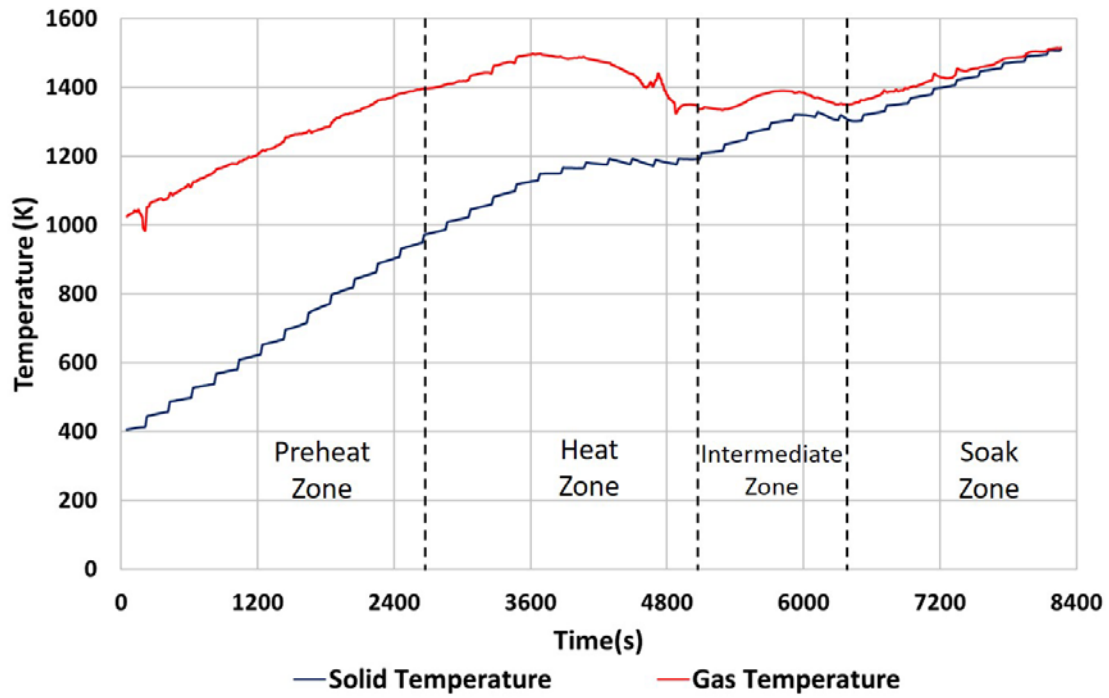
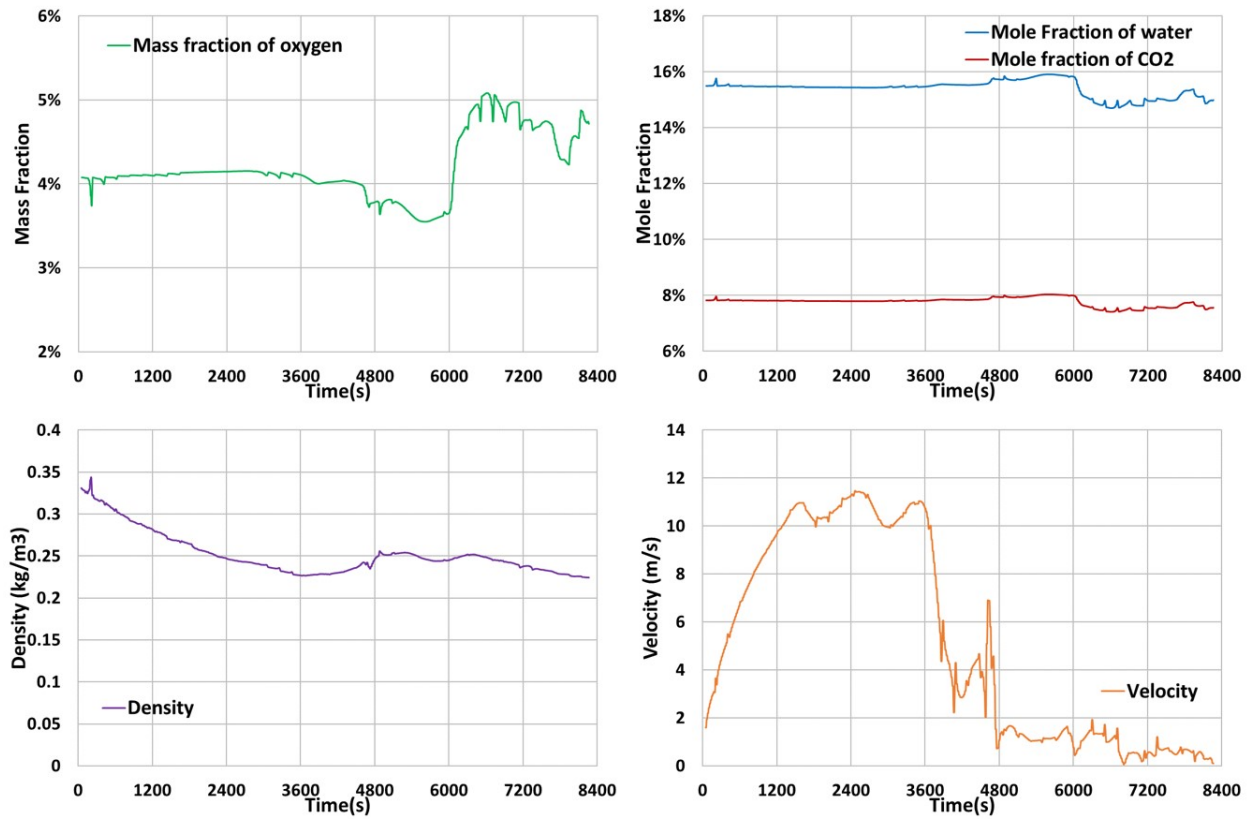Figure 5-1 Baseline case slab surface temperature

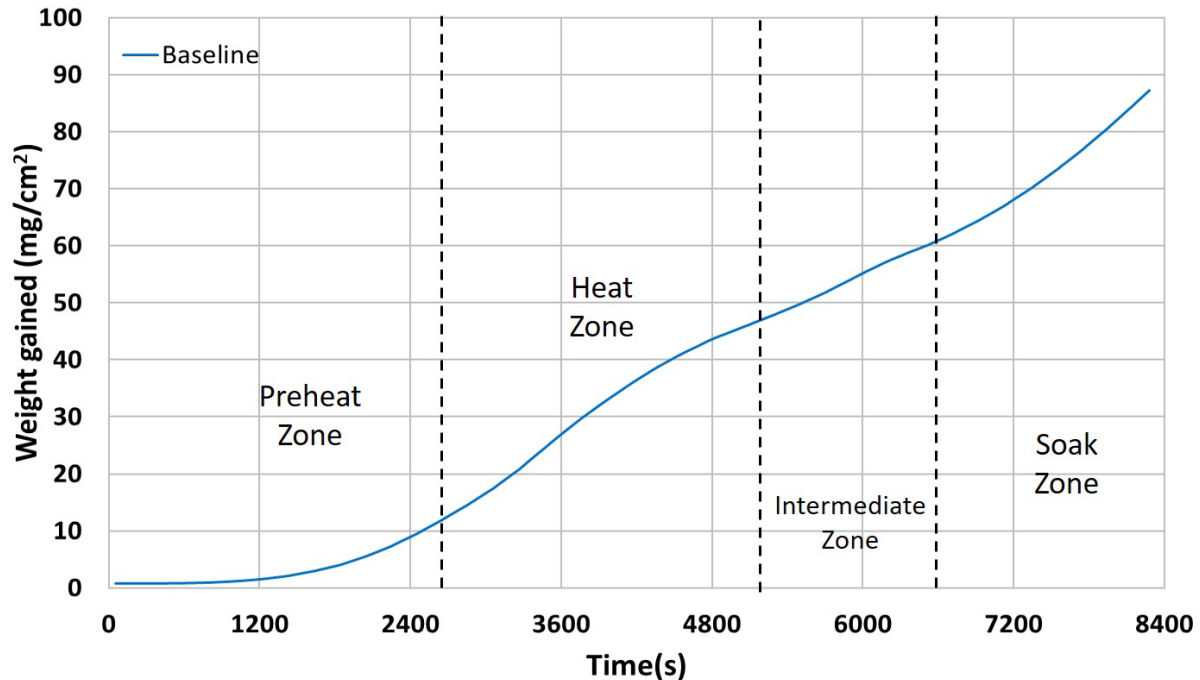Figure 5-2 Parameters of baseline case

Figure 5-3 Mass gained from scale in baseline case per unit area

It is easy to see that the scale formation rate is related to both gas temperature and slab temperature. Eventhough the slab only spends one third of the total reheating time in the preheat zone, only 14% of total scale formed in preheat zone. This is due to the low slab temperature and gas temperature in the preheat zone. Then the formation rate keep raising until discharged, but the raising of formation rate slowed down at two connection area of zones because of the low gas temperature at the area.

As shown in Figure 5-4, temperature distribution of slab surface is not uniform, so the scale formation at different positions of the slab are different. Six lines of data in are chosen to compute the scale formation rate at these positions. Results are shown in Figure 5-5.

For the top surface, scale formed at center line is less than both of two sides, this is because the temperature of sides can be higher when those parts are protrude out because of the slab distribution. At bottom surface, although those parts still protrude and have higher temperature, the beam with water cooling near sides reduced the temperature a lot, so the scale formation at left side do not obviously higher than centerline, but the effect of cooling is worse at the left side, so the scale formed at left side is more.
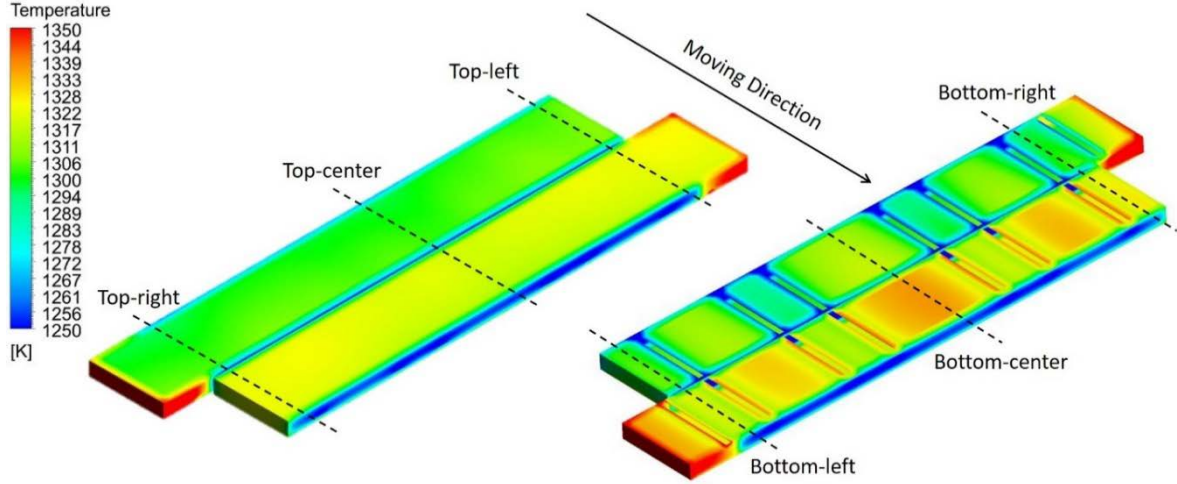
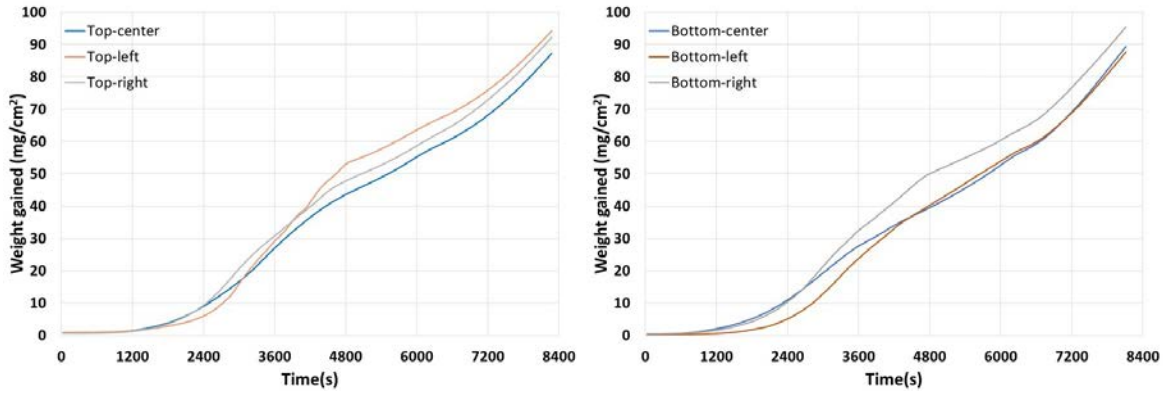Figure 5-4 Temperature distribution on two slab surfaces

Figure 5-5 Scale formation at different positions

5.2   Parametric study

In most of the improvement of gas injection, total gas flow rate is reduced to decrease heat wasted on heating up gas. To study the influence to scale formation of reduced gas flow rate, a group of parametric study is set. Considering that the total heat released by combustion is assumed as not changed, the gas temperature should change with gas flow rate. The average temperature of injected gas is measured as 627.8K. So the gas temperature should follow below equation:

$$(T_1 - 627.8K) \times \dot{m}_1 = (T_0 - 627.8K) \times \dot{m}_0 \qquad (5.1)$$

Subscript 0 means baseline and 1 means parametric study, T is the gas temperature and $\dot{m}$ is the mass flow rate. The density is also influenced through ideal gas law and the gas velocity is also

55

fixed using calculated new mass flow rate and density. For the study of decreased gas flow, three parametric case is computed, the flow rate percentage change of three parametric study cases are: case 1, -1%, case 2, -3%, and case 3, -5%. As shown in Figure 5-6, the trend is all the same but the formed scale increase with the increased temperature and decreased flow. Thus because with the temperature raising, the diffusion coefficient raised with the temperature and diffusion of iron ion enhanced, more iron ion transferred to the scale surface and accelerate the scale formation. Since this furnace is divided into 4 zones: preheat zone (PHZ), heat zone (HZ), intermediate zone (INTZ) and soak zone (SZ), 3 points between zones and the end point are chosen to calculate mass gained in each zones and whole process of cases, results are shown in Table 5-1

Table 5-1 Result of reduced-flow cases

WEIGHT GAINED IN	BASELINE	CASE #1	CASE #2	CASE #3
PHZ (mg)	12.66	12.95	13.57	14.24
Changing (%)	------	+2.3%	+7.2%	+12.5%
HZ (mg)	32.73	33.07	33.84	34.77
Changing (%)	------	+1.1%	+3.4%	+6.2%
INTZ (mg)	13.77	13.93	14.26	14.56
Changing (%)	------	+1.2%	+3.5%	+5.8%
SZ (mg)	28.10	28.47	29.22	29.98
Changing (%)	------	+1.31%	+3.97%	+6.68%
Whole Process (mg)	87.26	88.42	90.89	93.55
Changing (%)	------	+1.3%	+4.2%	+7.2%

For reducing gas flow by 1%, 3% and 5%, scale formation increased about 1.3%, 4.2% and 7.2%, according to Figure 5-6 and Table 5-1. The main increase of scale formation happens in preheat zone and soak zone. For the 5% flow reduction case, the scale formation increase in these two zones are 12.5% and 6.68%. Since scale formation is preferred to be avoided, controlled the reducing of gas flow of preheat and heat zone might help.

When the combustion of reheating furnace improved, the temperature of flame may increase. With a higher flame temperature and radiation heat transfer, total heat requirement decreased, and as a result, the temperature of the furnace gas decreased. To study the influence of decreased furnace gas temperature, case 4, 5 and 6 are set with the heat transferred to furnace gas

reduced by 1%, 3% and 5%, results are shown in Figure 5-7. Also, scale formation data of zones are shown in Table 5-2.
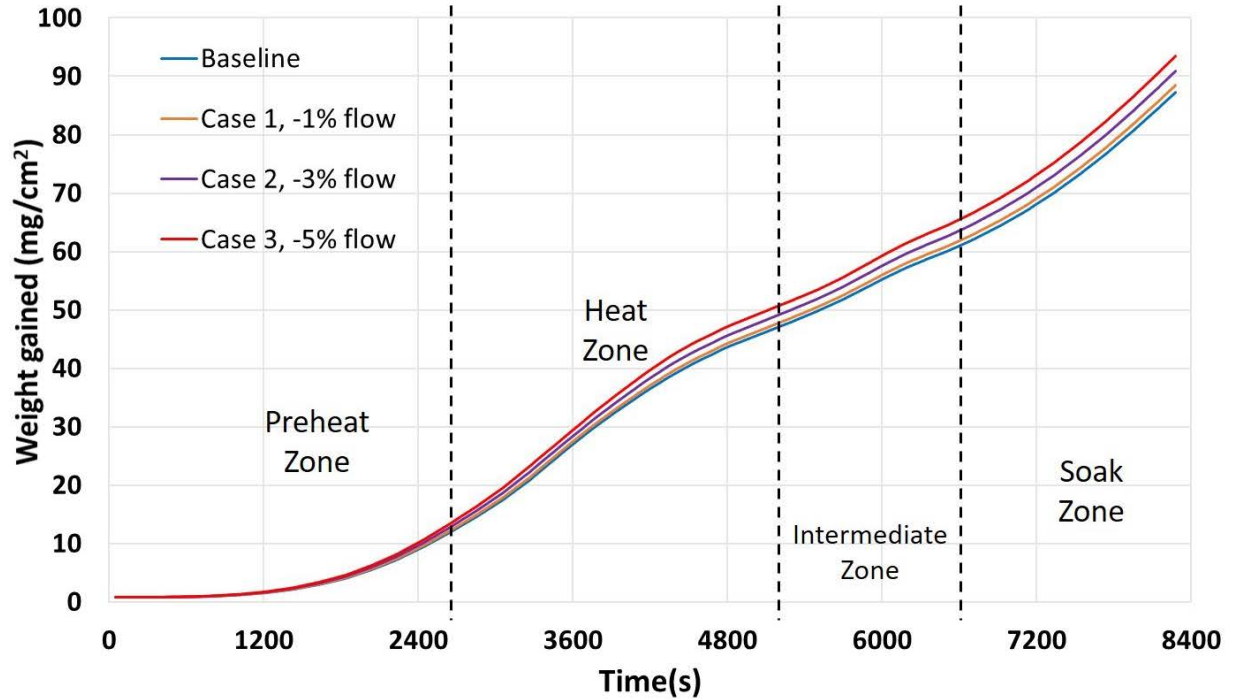

Figure 5-6 Result of reduced-flow cases

Table 5-2 Result of reduced-heat cases

WEIGHT GAINED IN	BASELINE	CASE #4	CASE #5	CASE #6
PHZ (mg)	12.66	12.37	11.82	11.28
Changing (%)	------	-2.3%	-6.7%	-10.9%
HZ (mg)	32.73	32.43	31.92	31.34
Changing (%)	------	-0.9%	-2.5%	-4.2%
INTZ (mg)	13.77	13.59	13.24	12.94
Changing (%)	------	-1.3%	-3.8%	-6.0%
SZ (mg)	28.10	27.73	26.98	26.25
Changing (%)	------	-1.33%	-3.99%	-6.60%
Whole Process (mg)	87.26	86.13	83.96	81.80
Changing (%)	------	-1.3%	-3.8%	-6.3%

Similar to the first group of parametric study, the result shows that the influence of gas temperature is larger in the preheat zone and heat zone. For the total scale formation during the process, the reduction of cases with 1%, 3% and 5% gas heated temperature decrease are 1.3%, 3.8% and 6.3%, which shows that the influence of temperature is not linear but decrease with the

gas temperature decrease. As mentioned before, the decreased scale formation rate with decreased temperature is because of the weakened iron ion transfer ability, since the relationship between iron ion diffusion coefficient and temperature is not linear but raise faster at higher temperature, the influence of temperature decreased at lower temperature can be explained.
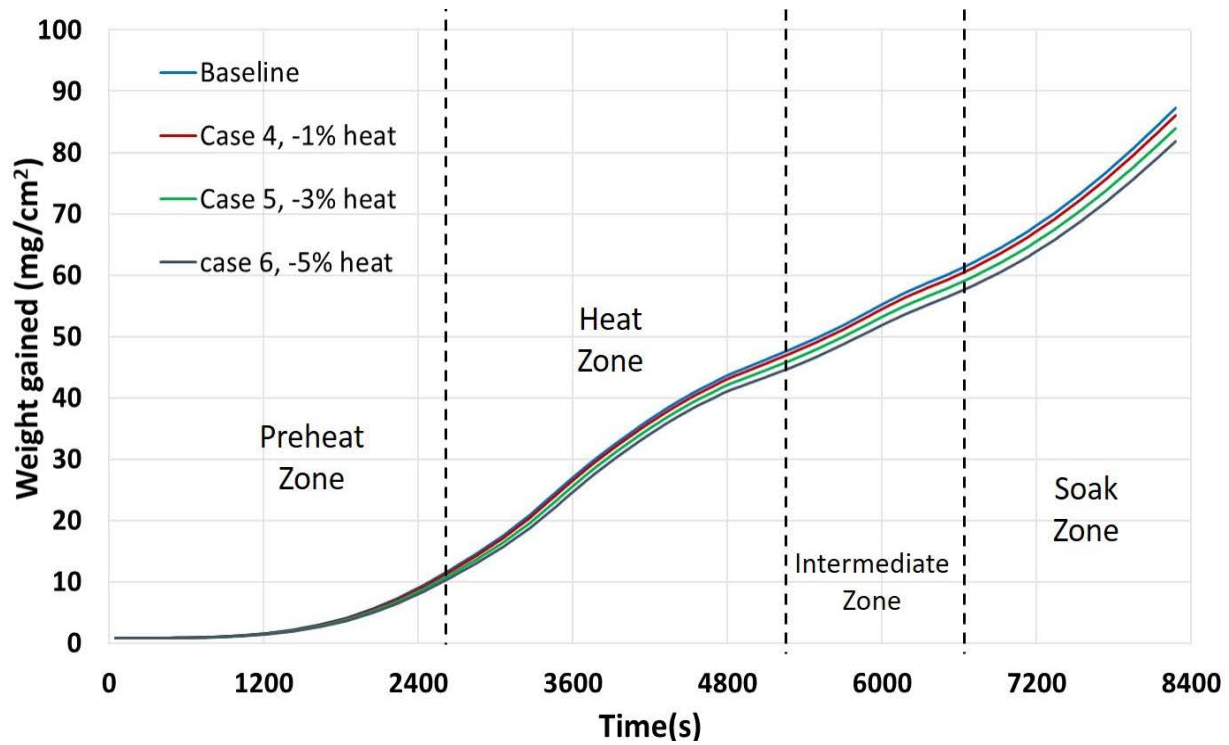

Figure 5-7 Result of reduced-heat cases

6. CONCLUSION

In this work a scale formation model using for numerical simulation of steel reheating process is developed. The scale formation model is used the computational fluid dynamics software ANSYS Fluent to solve the scale formation in both transient cases and steady-state cases. A calculator that can calculate scale thickness and mass growth use both data of two types of cases or industrial data is also developed. The model was developed base on the theory of low carbon steel oxidation, so it may not be adequate to cover the oxidation of high-carbon, high-alloy metal or pure iron. Also because of the incomputable scale separation, the accuracy of the model will decrease at temperatures below 950°C. The model is validated against experimental results from multiple researchers.

A four zone walking-beam reheating furnace case is used as the baseline case, the result shows the trend of scale formation during the reheating process. The scale formation rate raising with the slab surface temperature raising, this raising slow down when the gas temperature decrease. Because of the keeping raise of the formation rate, only 7.4% of the scale formed in the preheat zone and most of the scale formed in the soak zone, so improve the heat transfer efficiency and reduce the soak zone length might be a way that can reduce the scale formation.

Parametric studies explore the influence of gas flow and heat absorbed by gas, with the gas flow decreasing, the temperature raised and the scale formation increased around 1.5% with every 1% gas flow decrease, this value is increased with gas flow decreasing. For absorbed heat, around 1.5% scale mass dropped with 1% heated decreasing, and the ration is keep decreasing with the gas temperature decrease. In both parametric studies, preheat zone and heat zone scale formation are much easier to be influenced, the percentage changing of these two zones are 2 to 3 times of other zones, since scale formed in preheat zone is too less, the operation condition control of heat zone may have best efficiency of scale control.

REFERENCES

[1].   P. Mullinger and B. Jenkins. "Industrial and Process Furnaces: Principles, Design and Operation." Elsevier via Butterworth-Heinemann (2008) Hungary.

[2].   W. Weißbach. "Materials Science Structures, Properties, Testing." 17th ed. (2019) p. 76.

[3].   Z. Li, P. V. Barr, and J. K. Brimacombe. "Computer Simulation of the Slab Reheating Furnace." *Canadian Metallurgical Quarterly*, vol. 27, no. 3 (1988) pp. 187-196.

[4].   K. S. Chapman, S. Ramadhyani, and R. Viskanta. "Two-Dimensional Modeling and Parametric Studies of Heat Transfer in a Direct-Fired Furnace with Impinging Jets." *Combustion Science and Technology*, vol. 97, no. 1-2 (1994) pp. 99-120.

[5].   "Recent trends in the cost of computing." *AI IMPACTS*, (2017)

[6].   H. C. Hottel and A. F. Sarofim. "Models of Radiative Transfer in Furnaces." *Journal of Engineering Physics*, vol. 19, no. 3 (1970) pp. 1102-1114

[7].   J. G. Kim, K. Y. Huh, and I. T. Kim. "Three-dimensional analysis of the walking-beam-type slab reheating furnace in hot strip mills." *Numerical Heat Transfer: Part A: Applications*, vol. 38, no. 6 (2000) pp. 589-609.

[8].   Y. Yang, J. Kroeze, and M. A. Reuter. "Simulation of slab movement and transient heating in a continuous steel reheat furnace." *Progress in Computational Fluid Dynamics an International Journal*, vol. 4, no. 1 (2004) pp. 46-58

[9].   M. Huang, C. Hsieh, S. Lee, and C. Wang. "A Coupled Numerical Study of Slab Temperature and Gas Temperature in the Walking-Beam-Type Slab Reheating Furnace." *Numerical Heat Transfer, Part A: Applications*, vol. 54, no. 6 (2008) pp. 625-646.

[10].   Schluckner, C., C. Gaber, M. Demuth, S. Forstinger, R. Prieler, and C. Hochenauer. "CFD-model to predict the local and time-dependent scale formation of steels in air-and oxygen enriched combustion atmospheres." *Applied Thermal Engineering* 143 (2018): 822-835.

[11].   Liu, Xiang, Bethany Worl, Guangwu Tang, Armin K. Silaen, Jeffrey Cox, Kurt Johnson, Rick Bodnar, and Chenn Q. Zhou. "Numerical Simulation of Heat Transfer and Scale Formation in a Reheat Furnace." *steel research international* 90, no. 4 (2019): 1800385.

[12].   Worl, Bethany M. "Numerical Investigation of Combustion and Oxidation in a Steel Reheat Furnace." MS thesis., Purdue University Graduate School, 2019.

[13]. Darken, Lo S., and R. W. Gurry. "The system iron-oxygen. I. The wüstite field and related equilibria." *Journal of the American Chemical Society* 67, no. 8 (1945): 1398-1412.

[14]. Pettit, F. S., and J. B. Wagner Jr. "Transition from the linear to the parabolic rate law during the oxidation of iron to wüstite in CO-CO2 mixtures." *Acta Metallurgica* 12, no. 1 (1964): 35-40.

[15]. Turkdogan, E. T., W. M. McKewan, and L. Zwell. "Rate of oxidation of iron to wustite in water-hydrogen gas mixtures." *The Journal of Physical Chemistry* 69, no. 1 (1965): 327-334.

[16]. Grabke, H. J., K. J. Best, and A. Gala. "Sauerstoffübertragung aus CO_2-CO- und H_2O-H_2-Gemischen auf Metalle und Oxide." *Materials and Corrosion* 21, no. 11 (1970): 911-916.

[17]. Sachs, K., and C. W. Tuck. "Scale Growth during Re-heating Cycles." *Materials and Corrosion* 21, no. 11 (1970): 945-954.

[18]. Deich, J., and F. Oeters. "Zur Verzunderung von Weichstahl in Stickstoff-Kohlendioxid-Gemischen mit geringen Sauerstoffzusätzen." *Materials and Corrosion* 24, no. 5 (1973): 365-371.

[19]. Abuluwefa, Husein. "Scale formation in a walking-beam steel reheat furnace." (1992).

[20]. Abuluwefa, H. T., R. I. L. Guthrie, and F. Ajersch. "Oxidation of low carbon steel in multicomponent gases: Part I. Reaction mechanisms during isothermal oxidation." *Metallurgical and Materials Transactions A* 28, no. 8 (1997): 1633-1641.

[21]. Abuluwefa, H. T., R. I. L. Guthrie, and F. Ajersch. "Oxidation of low carbon steel in multicomponent gases: Part II. Reaction mechanisms during reheating." *Metallurgical and Materials Transactions A* 28, no. 8 (1997): 1643-1651. .

[22]. Chen, Rex Y., and W. Y. D. Yuen. "Short-time oxidation behavior of low-carbon, low-silicon steel in air at 850–1180℃: II. Linear to parabolic transition determined using existing gas-phase transport and solid-phase diffusion theories." *Oxidation of metals* 73, no. 3 (2010): 353-373.

[23]. Giddings, Robert A., and Ronald S. Gordon. "Review of Oxygen Activities and Phase Boundaries in Wustite as Determined by Electromotive-Force and Gravimetric Methods." *Journal of the American Ceramic Society* 56, no. 3 (1973): 111-116.

[24]. Chen, W. K., and N. L. Peterson. "Effect of the deviation from stoichiometry on cation self-diffusion and isotope effect in wüstite, $Fe_{1-x}O$." *Journal of Physics and Chemistry of Solids* 36, no. 10 (1975): 1097-1103

[25]. Yin, H., S. L. I. Chan, W. Y. D. Yuen, and D. J. Young. "Temperature Effects on the Oxidation of Low Carbon Steel in N_2-H_2-H_2O at 800–1200 °C." *Oxidation of metals* 77, no. 5 (2012): 305-323.

[26]. Lee, V. H. J., B. Gleeson, and D. J. Young. "Scaling of carbon steel in simulated reheat furnace atmospheres." *Oxidation of metals* 63, no. 1 (2005): 15-31.

[27]. Abuluwefa, Husein. "Characterization of oxides (scale) growth of low carbon steel during reheating." (1996).

[28]. Chen, R. Y., and W. Y. D. Yuen. "Effects of the presence of water vapour on the oxidation behaviour of low carbon–low silicon steel in 1 % O_2–N_2 at 1073 K." *Oxidation of metals* 79, no. 5 (2013): 655-678.

[29]. Yurek, Gregory J., John P. Hirth, and Robert A. Rapp. "The formation of two-phase layered scales on pure metals." *Oxidation of Metals* 8, no. 5 (1974): 265-281.

[30]. Dieckmann, R., and H. Schmalzried. "Defects and cation diffusion in magnetite (I)." *Berichte der Bunsengesellschaft für physikalische Chemie* 81, no. 3 (1977): 344-347.

[31]. Garnaud, G., and Robert A. Rapp. "Thickness of the oxide layers formed during the oxidation of iron." *Oxidation of Metals* 11, no. 4 (1977): 193-198.

[32]. Abuluwefa, H. T. "Kinetics of high temperature oxidation of high carbon steels in multi-component gases approximating industrial steel reheat furnace atmospheres." *Lecture notes in engineering and computer science* (2012).

[33]. Grønvold, Fredrik, Svein Stølen, Pauline Tolmach, and Edgar F. Westrum Jr. "Heat capacities of the wüstites $Fe_{0.9379}O$ and $Fe_{0.9254}O$ at temperatures T from 5 K to 350 K. Thermodynamics of the reactions: xFe (s) $+$ (1/4) Fe_3O_4 (s) $=$ $Fe_{0.7500+x}O$ (s) $=$ $Fe_{1-y}O$ (s) at T≈ 850 K, and properties of $Fe_{1-y}O$ (s) to T= 1000 K. Thermodynamics of formation of wüstite." *The Journal of Chemical Thermodynamics* 25, no. 9 (1993): 1089-1117.

[34]. Takeda, Mikako, Takashi Onishi, Shouhei Nakakubo, and Shinji Fujimoto. "Physical properties of iron-oxide scales on Si-containing steels at high temperature." *Materials transactions* 50, no. 9 (2009): 2242-2246.

[35]. Wikström, Patrik, Yang Weihong, and Wlodzimierz Blasiak. "The influence of oxide scale on heat transfer during reheating of steel." *steel research international* 79, no. 10 (2008): 765-775.

[36]. Abuluwefa, H., R. I. L. Guthrie, and F. Ajersch. "The effect of oxygen concentration on the oxidation of low-carbon steel in the temperature range 1000 to 1250 C." *Oxidation of Metals* 46, no. 5 (1996): 423-440.

[37]. Howard, J. R., and A. E. Sutton. "An analogue study of heat transfer through periodically contacting surfaces." *International Journal of Heat and Mass Transfer* 13, no. 1 (1970): 173-183.

[38]. Paidassi, J. "The kinetics of the air oxidation of iron in the range 700-1250-degrees-C." *Acta Metallurgica* 6, no. 3 (1958): 184-194.

[39]. Chase Jr, M. W. "NIST-JANAF Thermochemical Tables-Fourth Editions, Parts 1 and 2." (1998).

[40]. Akiyama, Tomohiro, Hiromichi Ohta, Reijiro Takahashi, Yoshio Waseda, and Jun-ichiro Yagi. "Measurement and modeling of thermal conductivity for dense iron oxide and porous iron ore agglomerates in stepwise reduction." *ISIJ international* 32, no. 7 (1992): 829-837.